

**GROWTH AND SIMULATION STUDY OF GAN ON V-
GROOVE PATTERNED SILICON (100) SUBSTRATES AND
ITS APPLICATIONS**

LI SHIJU

(B.Eng (Hons.), NUS)

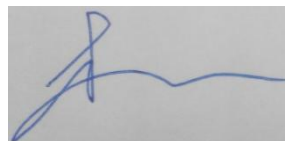
**A THESIS SUBMITTED
FOR THE DEGREE OF MASTER OF ENGINEERING
DEPARTMENT OF ELECTRICAL AND COMPUTER ENGINEERING
NATIONAL UNIVERSITY OF SINGAPORE**

2016

DECLARATION

I hereby declare that this thesis is my original work and it has been written by me in its entirety. I have duly acknowledged all the sources of information which have been used in the thesis.

This thesis has also not been submitted for any degree in any university previously.

A rectangular box containing a handwritten signature in blue ink. The signature is stylized and appears to be 'Li Shiju'.

Li Shiju

August 2016

Acknowledgements

No man is an island. I would like to take this opportunity to thank those whose support and help are indispensable for the completion of this master thesis.

First and foremost, I would like to express my sincere gratitude to my supervisor, Professor Chua Soo Jin, for his kind and invaluable guidance in my master study. I am grateful for the opportunity introduced by Prof. Chua to work as an attachment student at IMRE, A*Star. The learning experience is truly fulfilling.

I would like to express special thanks to Dr. Kwadwo Konadu Ansah-Antwi, for guiding me and training me to use MOCVD. I would like to thank Dr. Liu Hongfei and Dr. Wang Benzong of IMRE, for their patience and guidance in having many discussions with me on experiment and simulation.

One of the greatest things during my master study is that I have made great friends. I would like to thank my coursework classmates Mei Shengtao, Du Fang (Quantum mechanics study group), Kong Lingyu, Sachin, Wu Mengxue (MicroE processing) Shi Qiongfeng, Lei Dian, Yang Rui, Sun Ruize. The time we had discussing quantum mechanics and photonics, and stressful preparations before exams are all wonderful memories.

I am grateful that I have met great seniors in my supervisor's laboratory. I would like to thank Li Chengguo, Huang Jian, Zhang Li, Tang Jie, Hou Haowen, Deng Liyuan, Ho Jian Wei, and Guo Yilin, for your companion and friendship. To Liu Yi, listening to Mark Knopfler's guitar solos is always a joyful thing to do in our office. I will also remember our regular trips to our favorite Indian food restaurant, where many interesting conversations took place. To Zhang Chen, the time we sang "Heart of Gold" together is so memorable. Thank you for hosting me at Boston during MRS Conference. The walks we had in Boston and MIT have given me a precious time of deep thought and soul searching. I would like to extend my sincere thanks to two lovely and warm-hearted couples, Chen Zhi and Tingting, Cheng Kun and Lulu, whom I shared an apartment with.

I want to thank my girlfriend, Dieling, for staying by my side especially during difficulties and harsh times. Our trip to Bali is full of adventures and fun. I wish we could travel to more places in the future, and enjoy our life journey together.

I want to thank my dearest parents and my elder brother. I have been away from home for more than a decade, and I do miss you all. I wish we could spend more time together in the future.

Table of Contents

Title page.....	I
Acknowledgements.....	II
Summary	VII
List of Tables.....	X
List of Figures	XI
Chapter 1. Introduction.....	1
1.1. Motivation for GaN-on-Si.....	1
1.1.1. Background.....	1
1.1.2. Challenges of GaN-on-Si.....	5
1.1.3. Development history and market prospects of GaN-on-Si technology	9
1.2. Research objective.....	10
1.3. Organization of the thesis.....	10
Chapter 2 MOCVD growth of GaN on Si (100) substrates patterned with V- grooves	12
2.1. Overview of GaN growth in MOCVD.....	12
2.2. MOCVD equipment.....	13
2.2.1. Precursors.....	15
2.2.2. GaN growth process.....	15
2.3. Overview of GaN growth on patterned silicon substrate	18
2.3.1. Processing steps	18
2.3.2. Growth of GaN on silicon substrates with various crystalline orientations	20
2.4. Growth of GaN in EMCORE D180 MOCVD	27
2.4.1. Growth equipment	27
2.4.2. Substrate preparation	27
2.4.3. Substrate patterning	28
2.4.4. MOCVD growth of GaN	29

2.4.5. characterization	31
Chapter 3 Simulation of GaN growth on Si (100) substrates patterned with V-grooves	36
3.1. Motivation for MOCVD simulation.....	36
3.2. Review of MOCVD growth of GaN	39
3.2.1. Reactions leading to growth of GaN.....	39
3.2.2. Review of MOCVD design.....	44
3.3. Simulation of GaN growth on Si (100) substrates patterned with V-grooves in COMSOL	46
3.3.1. Setup of COMSOL simulation.....	46
3.3.2. COMSOL simulation results.....	53
3.3.3. COMSOL simulation results.....	55
3.3.3.1. Velocity magnitude distributions.....	55
3.3.3.2. Pressure distributions.....	58
3.3.3.3. Temperature distributions.....	60
Chapter 4 Proposed integration of single-photon emitter with optical fiber in cascaded V-grooves on Si (100) substrate	66
4.1. Motivation	66
4.1.1. Overview.....	66
4.1.2. Introduction to non-classical light generation.....	69
4.1.2.1. Non-classical light	69
4.1.2.2. Single photon source	73
4.2. Area-selective quantum well intermixing and quantum dot fabrication	75
4.3. Proposed structure	79
4.4. Simulation of proposed single-photon emitter with optical fiber in cascaded V-grooves on Si (100) substrate	82
4.4.1. Fabrication of QD by QWI	82
4.4.2. Coupling with silicon waveguide.....	86
Chapter 5 Conclusion and future work	88
5.1 Conclusion.....	88
5.2 Future work	90
Bibliography.....	92

Appendices	99
A.1 Biography	99
A.2 Publication list	99
A.3 Participation in international conference	99
A.4 Setup in COMSOL	99
A.5 Setup of InGaN / GaN QW in SILVACO	101

Summary

In this thesis, growth and simulation study of gallium nitride on silicon (111) facets of V-grooves patterned on silicon (100) substrates are performed. The theme of GaN growth on silicon substrate is widely studied, as it enables the integration of III-V based electronic and optoelectronic devices with Si-CMOS-based logic devices.

In order to grow GaN on Si (100) substrate, V-grooves are patterned on Si (100) substrate to expose the Si (111) facets. The growth is performed in an EMCORE D180 MOCVD system. Three types of substrates are prepared, with their V-grooves placed at 0° , 45° and 90° to the precursor flow direction. It is found that single-facet growth of GaN is achieved when V-grooves are placed perpendicular to precursor flow. For 45° placement, two triangular prisms which differ in size are obtained on the two Si (111) facets. For the case of 0° placement, no growth is observed. This observation could be used to replace the current method of masking one Si (111) facet by Glancing Angle Deposition prior to GaN growth to achieve single-facet growth of GaN within V-grooves. It can simplify the growth process.

A simulation study is performed in COMSOL software to elucidate the impact of V-grooves on laminar flow and heat transfer within the reactor. The distributions of precursor velocity, pressure and temperature within the reactor chamber are simulated. Due to mesh size limit of COMSOL, the V-grooves simulated will have larger dimensions than those used in the experiment. It is found that velocity of precursor over the V-grooves would be slower than that over the flat substrate. Furthermore, the presence of V-grooves on Si substrate will cause the pressure over one of the two facets to increase. This increase in pressure is related to an increase in gas flux and adsorption rate through the Hertz-Knudsen Equation. On the contrary, the presence of V-grooves has little impact on temperature distributions.

Lastly, a novel single-photon emitting and coupling structure within a V-groove of Si (100) substrate is proposed and simulated. The proposed structure consists of an InGaN / GaN quantum dot within a single quantum well (SQW) based light-emitting diode structure in a smaller V-groove, and an optical fiber in a bigger cascaded V-groove. In order to create a QD within the SQW, selective quantum well intermixing (QWI) is proposed. A small QW region designed to be non-intermixed is covered by circular patch-shape layer of SiO₂ with diameter of 200 nm. Then, the QW is covered by a Molybdenum:SiO₂ cap layer. Simulation in SILVACO has revealed that the bandgap in the selectively intermixed region with diffusion length of 10 Å increases by 20 meV. A QD region is obtained under the SiO₂ patch layer with a smaller bandgap. In order to couple the emitted photons, a

single-mode optical fiber is proposed to be embedded within a larger V-groove cascaded to the smaller V-groove. This structure would provide a predictable and controllable way to collect photons emitted.

List of Tables

Table 1-1. Summary of silicon and gallium nitride's important parameters at 300K. Data extracted from online material catalog <i>www.ioffe.ru</i>	4
Table 1-2. Lattice constants and thermal expansion coefficients of silicon, gallium nitride, sapphire and aluminum nitride. The values are taken from review article.	6
Table 2-1. Specifications for Emcore D180 TurboDisc vertical reactor.....	14
Table 3-1. Gas phase reactions of GaN growth involving decomposition of TMG.	42
Table 3-2. Gas phase reactions of GaN growth involving adduct formation and oligomerization.	43
Table 3-3. Surface reactions for GaN growth in MOCVD.	44
Table 4-1. Classification of light based on photon arrival intervals, and corresponding values of second-order correlation functions and classical descriptions. (Fox, 2006).....	70

List of Figures

Figure 1-1. Diagram for frequency and power applicability of semiconductor materials. (Li <i>et al.</i> , 2010)	4
Figure 2-1. Schematics of variants of MOCVD reactors: (a) rotating-disk vertical reactor (b) horizontal reactor (c) planetary reactor. Blue circles and rectangles represent wafers placed on susceptor.....	14
Figure 2-2. Two-step growth flow of GaN on sapphire.....	16
Figure 2-3. Comparison of growth processes for GaN on (a) sapphire and (b) silicon. ...	16
Figure 2-4. Schematic of Glancing Angle Deposition system (GLAD).....	20
Figure 2-5. Silicon atomic structure as viewed from different crystalline directions.....	22
Figure 2-6. Various planes in GaN unit cell.....	23
Figure 2-7. Process flow for growth of GaN on 7° off-cut Si (100) substrate.....	25
Figure 2-8. Process flow for growth of GaN on Si (113) substrate.....	26
Figure 2-9. Process flow for growth of GaN on Si (110) substrate.....	26
Figure 2-10. Schematic illustrating the processing steps for patterning V-grooves on Si (100) substrate for GaN growth.....	29
Figure 2-11. Layout of susceptor loaded with V-groove-patterned Si (100) substrates, with V-grooves aligning in 0°, 45°, 90° to precursor flow (red arrow) for Samples A (purple grooves), B (orange grooves) and C (green grooves) respectively. \vec{v} denotes the direction of precursor flow. \vec{n} denotes the normal direction to V-grooves.....	30
Figure 2-12. Schematic illustrating the stack of material layers grown on Si (111) facets of V-grooves patterned on Si (100) substrates.....	31
Figure 2-13. SEM images of (a) Sample A (b) Sample B (c) Sample C.....	32
Figure 2-14. SEM image of Sample C after a growth time of 20 minutes.....	33
Figure 2-15. PL spectra of GaN grown in Sample C.....	34
Figure 3-1. Gas-phase reaction pathways for GaN growth in MOCVD. Adapted from (Parikh & Adomaitis, 2006).....	40
Figure 3-2. Gas flow visualization in a rotating disk MOCVD reactor chamber. (Breiland & Evans, 1991)	46
Figure 3-3. Simulation flow chart using COMSOL to study the growth of GaN on V-groove-patterned Si (100) substrates.....	47
Figure 3-4. Setup in Laminar Flow Interface.....	50
Figure 3-5. Setup in Heat Transfer in Fluids Interface of COMSOL.....	52
Figure 3-6. Geometry setup for reactor chamber loaded with substrate patterned with V-grooves.....	55
Figure 3-7. Velocity magnitude distribution within reactor chamber loaded with flat substrates.....	56
Figure 3-8. Velocity magnitude distribution within reactor chamber loaded with V-grooves-patterned substrate.....	57
Figure 3-9. Pressure distributions in reactor chamber loaded with (a) flat and (b) V-groove-patterned substrates.....	58

Figure 3-10. Temperature distribution (a) and contour plot (b) in reactor chamber loaded with flat substrates.	61
Figure 3-11. Temperature distribution (a) and contour plot (b) in reactor chamber loaded with V-groove patterned substrates.	62
Figure 3-12. For hypothetical study of higher specific heat capacity of precursor, temperature distribution (a) and contour plot (b) in reactor chamber loaded with flat substrates.....	63
Figure 3-13. For hypothetical study of higher specific heat capacity of precursor. Temperature distribution (a) and contour plot (b) in reactor chamber loaded with V-grooves-patterned substrates.	64
Figure 4-1. Proposed device structure consisting of a single-photon source and an optical fiber, embedded within cascaded V-grooves on Si (100) substrate.	68
Figure 4-2. (a) Semipolar (1-101) InGaN/GaN LED grown on Si (111) facets of V-grooves patterned on Si (100) substrate. (b) Reference LED on polar (0001) plane. (Reuters <i>et al.</i> , 2015).....	69
Figure 4-3. Illustration for photon streams in different types of light sources.....	70
Figure 4-4. Hanbury Brown and Twiss setup for measuring second-order correlation function.	72
Figure 4-5. Single-photon emitter structure based on self-assembled quantum dots with electrical pumping. (Yuan <i>et al.</i> , 2002)	74
Figure 4-6. Proposed detailed layer stack grown on Si (111) facet of V-groove.....	80
Figure 4-7. Proposed cap layer depositions on semi-polar InGaN / GaN SQW fabricated on Si (111) facet of V-groove.	81
Figure 4-8. Proposed cap layer depositions on polar InGaN / GaN SQW fabricated on Si (111) facet of V-groove.	82
Figure 4-9. Indium composition profile for as-grown QWs (blue), and intermixed QWs (red).....	84
Figure 4-11. Single-mode optical fiber core placed within V-groove patterned on Si (100) substrate.	86

Chapter 1. Introduction

1.1. Motivation for GaN-on-Si

The discovery and utilization of semiconductor materials have led to vast developments in various scientific and industrial fields. Semiconductor materials could be classified into single element semiconductors and compound semiconductors. Silicon, the nearly ubiquitous single-element semiconductor, is the foundation for the current integrated circuit technology. Among compound semiconductors, gallium nitride (and its alloys with indium and aluminum) is an important family of semiconductors for optoelectronics and switching devices. The effort of growing gallium nitride on silicon (GaN-on-Si) aims to bridge the best of the two worlds, and realize the integration of silicon electronics and compound semiconductor devices. This thesis would focus on selective-area growth of GaN on silicon (100) substrate patterned with V-grooves. Firstly, growth experiments are performed using EMCORE D180 MOCVD system. Then, simulation of growth dynamics is performed in COMSOL software environment.

1.1.1. Background

Silicon's ubiquitous usage in the semiconductor industry stems from its distinct properties. It has vast abundance in nature, making up 25.7% by weight of the earth crust. Silicon could be relatively easily extracted from compounds using the

Czochralski process. Moreover, the oxide form of silicon could be grown with high quality on silicon, forming a Si / SiO₂ interface that consists of a low number of traps. This high quality Si / SiO₂ interface defines a higher upper boundary of the active channel of CMOS transistor. On the other hand, silicon's limitations include an indirect bandgap, which hinders its applications in optoelectronic devices. Its relatively small bandgap of 1.11 eV also makes it unsuitable for high frequency and high power switching devices.

A compound semiconductor is composed of elements from more than one group of the periodic table. Among them, III-V semiconductors have a number of beneficial properties. Firstly, they are widely used in optoelectronic devices. Among them, conventional cubic III-V semiconductors such as arsenides and phosphides exhibit high efficiency in the infrared to red spectrum when used in light-emitting diodes (LED), although towards higher energy the bandgap becomes indirect and efficiency drastically drops. On the contrary, III-V nitride semiconductors and their alloys possess direct bandgap across the whole compositional range from AlN to InN. The wavelengths of light corresponding to their bandgaps could cover the whole visible spectrum. This allows them to be used in full-spectrum light emitting diodes and laser diodes. The current industrial production of LEDs and laser diodes use InGaAsP system or InAlGaN system.

Secondly, III-V semiconductor materials have excellent electron transport properties under both high field and low field. They also exhibit ultrahigh

switching speeds at low supply voltages. Figure 1 below shows the frequency and power operating range of various semiconductor materials. III-V semiconductors such as gallium nitride and gallium arsenide could be used for high power and high frequency applications. These properties enable III-V materials to be used in high electron mobility transistor (HEMT) and wireless infrastructure. For example, high electron mobility of GaAs and InP enables them to be implemented for transistors operating above 100 GHz. Gallium nitride's wide bandgap at 3.4 eV makes it a suitable candidate for high voltage and high power switching devices. High power and high frequency transistors based on III-V semiconductors possess strategic significance, as they are important components for military and space applications.

One constraint faced by III-V semiconductors is the expensive and size-constrained substrates. For gallium nitride, the mainstream substrates currently used are sapphire substrate with low temperature AlN buffer layer, or silicon carbide substrate (SiC). Growth of GaN on planar silicon substrate has also been reported in the literature (Mo *et al.*, 2005), although many complications in the growth process such as large lattice mismatch and melt-back etching make it unsuitable for industrial production (Wan *et al.*, 2001). Sapphire and silicon carbide substrates are only available in smaller sizes of 2 or 4 inches, whereas silicon substrates are available in size of 6 or 12 inches. Current lack of large sapphire and silicon carbide wafers put constraints on wafer expansion and further

reduction in the cost of LEDs. The advantages and disadvantages of silicon and III-V semiconductors are summarized in the Table 1 below. (Li *et al.*, 2010)

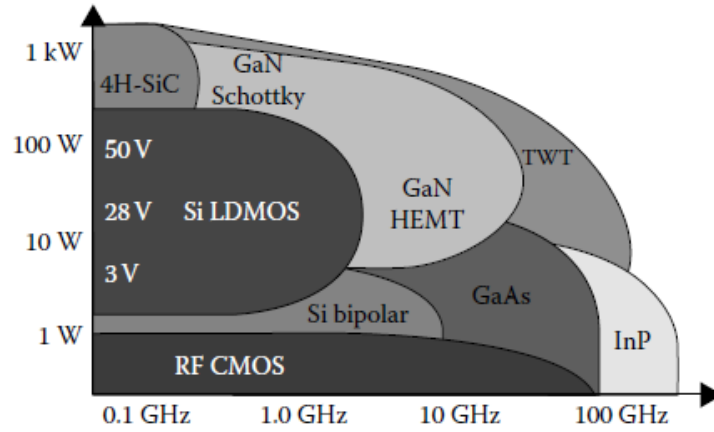


Figure 1-1. Diagram for frequency and power applicability of semiconductor materials. (Li *et al.*, 2010)

	Silicon	GaN
Bandgap (eV)	1.1	3.49
Electron Mobility (cm ² /Vs)	≤ 1400	990 - 2200
Critical breakdown field (MV/cm)	0.3	3.3
Saturated electron drift velocity (x10 ⁷ cm/s)	1.0	2.5

Table 1-1. Summary of silicon and gallium nitride's important parameters at 300K. Data extracted from online material catalog www.ioffe.ru.

Among III-V semiconductors, gallium nitride's wide and direct bandgap makes it an important material for switching and optoelectronic devices. Growth of gallium nitride on silicon (GaN-on-Si) is an attempt to bridge the technological advantages of gallium nitride and silicon semiconductors. Silicon and gallium

nitride have different technical advantages, and could complement each other when integrated together. When used as substrate, silicon could provide a mature and sizable integration platform with cost advantages. Large silicon wafers in sizes of 6 inches or larger are available. Furthermore, GaN-on-Si technology could enable the fabrication of GaN-based switching devices or photonic devices on silicon, and their integration with CMOS electronic devices. Such integration could increase the density of devices on wafer. Moreover, the prospects of GaN-on-Si are not only limited to integration at the device level, but also on the material level. For example, gallium nitride and other III-V materials such as InSb are investigated to replace the silicon channel in MOSFETS, in order to increase the speed of switching.

1.1.2. Challenges of GaN-on-Si

The attempt of growing gallium nitride on silicon comes with inherent difficulties due to mismatch in material properties.

(a) Mismatch in lattice constants and thermal expansion coefficients

In Table 2 below, it summaries the lattice constants and thermal expansion coefficients (TEC) of silicon, gallium nitride, sapphire and aluminum nitride. There exists a 17% mismatch in lattice constants of Si and GaN. When the lattice mismatch between two materials exceeds 7%, edge dislocations and defects would be formed and the material system would be strained. (Li *et al.*, 2010) One serious consequence of such mismatch is the formation of cracks when the gallium nitride epilayer thickness exceeds 1 μm . Furthermore, the stress induced

within crystal due to lattice mismatch would cause the wafer to bend, and pose serious difficulties for subsequent photolithography processes . Thus, the control of defects is crucial in heteroepitaxial growth of gallium nitride on silicon.

The mismatch in thermal expansion coefficients between silicon and gallium nitride is 115%. During the cooling processes from growth temperature in the range of 700 to 1000°C to room temperature, epitaxial gallium nitride film and silicon substrate will undergo different extents of contraction, which might cause the grown film to crack.

Material	GaN	Si	Sapphire	AlN
Lattice constant (Å)	a=3.189 c=5.185	a=5.431	a=4.759 c=12.991	a=3.112 c=4.982
Lattice mismatch	w.r.t GaN	17%	-16%	-2.5%
Thermal expansion coefficient (10^{-6}K^{-1})	5.59 (a) 3.17 (c)	2.6	7.30 (a) 8.50 (c)	5.27 (a) 4.15 (c)
Thermal expansion mismatch	w.r.t GaN	-115%	23.4%	-34.7%

Table 1-2. Lattice constants and thermal expansion coefficients of silicon, gallium nitride, sapphire and aluminum nitride. The values are taken from review article.

To overcome the problems arising from mismatches in lattice constants and TECs, various methods of stress management have been reported. The cracking of nitrides on Si could be mitigated by substrate patterning or stress compensation. (Krost & Dadgar, 2002) For GaN, the method of growing an intermediate buffer layer in between gallium nitride and silicon is widely used to prevent cracks and

reduce defects in gallium nitride. Candidates for buffer layers include low temperature GaN buffer layer, metal Al pre-deposition, and the most used aluminum nitride.

The reasons for using AlN as a preferred buffer layer are two-fold. Firstly, a AlN buffer layer could prevent direct contact between Ga atoms with Si, which reacts easily with each other (Ishikawa *et al.*, 1998). Secondly, AlN buffer layer in between silicon and GaN could cause the nature of strain between them to switch from tensile to compressive. This could help reduce cracks in gallium nitride. For mitigating the mismatch in thermal expansion coefficients, the use of buffer layer is not effective, as the silicon substrate is much thicker than the buffer layer and dominates the extent of thermal expansion or contraction.

Comparing to growth on sapphire substrate, growth of GaN on silicon substrate requires more steps to ensure crystal quality. Firstly, the oxide layer on top of the silicon substrate should be removed. This can be done by using dry etching technique and then an immersion in diluted HF solution. Additionally, after the growth of AlN buffer layer, an intermediate layer of AlGaN or multiple GaN/AlGaN superlattice needs to be grown preceding GaN growth to ensure a smooth transition from AlN to GaN.

(b) Selective area growth and lateral epitaxial overgrowth

Selective area growth (SAG) of gallium nitride on silicon refers to constraining the growth on certain crystalline planes patterned on the substrate. It is a promising method to grow high quality GaN having lower dislocation density with release of thermal stress on silicon substrate. Lateral epitaxial overgrowth (ELO) is an extension of SAG, by allowing crystal in adjacent growth areas to coalesce and form a flat surface. When SAG or ELO is performed on patterned substrates, masking of one or more facets with silicon oxide or nitride by angle electron beam deposition is required to ensure growth of AlN and GaN on the desired facet along the (0001) axis. For example, when GaN is grown on Si (100) substrates patterned with V-grooves, one of the V-groove sidewalls needs to be masked to avoid collision of crystals on the two facets. The masking step further complicates the processing flow of GaN-on-Si, and requires the use of angle electron beam deposition setup. The second chapter of this thesis would be devoted to propose a method of manipulating the relative direction of V-grooves on Si (100) substrate to precursor flow, in order to achieve single facet growth of GaN without masking the other facet.

(c) Other difficulties

During the growth of GaN on silicon in H₂ ambient, silicon might outgas into GaN layer, and result in an unintentional n-doping. This would pose difficulties for p-doping in device fabrication. Moreover, while there is continuing effort to develop GaN-on-Si technology, we have to be aware that there is a continuing effort in growing larger sapphire, silicon carbide, or even GaN native substrates.

Nonetheless, GaN-on-Si technology could provide benefits other than substrate cost savings, for example improving the performance of switching devices.

1.1.3. Development history and market prospects of GaN-on-Si technology

The first LED based on GaN-on-Si dated back to late 1990s, when IBM researchers utilized Molecular Beam Epitaxy (MBE) method for growth. (Guha & Bojarczuk, 1998) To reduce density of cracks in thick GaN layer, low-temperature buffers layers were developed. (Dadgar *et al.*, 2000) There are also reports on further improving the LED performance in the green light region. (Reuters *et al.*, 2014) (Reuters *et al.*, 2015) Recently, optically pumped lasing has been achieved from InGaN / GaN quantum wells fabricated on silicon (001) substrate. (Kushimoto *et al.*, 2015)

The potential market for GaN-on-Si lies in two fields, namely light-emitting diodes (LEDs) and power electronics. According to a market survey conducted by Yole Development, the market penetration rate for silicon substrate for LED applications is forecasted to increase to 5% by 2020. For power devices, GaN-on-Si power devices is forecasted to make up 1.5% of overall power substrate volume by 2020. ¹

¹ "GaN-on-silicon enabling GaN power electronics, but to capture less than 5% of LED making by 2020." http://www.semiconductor-today.com/features/PDF/SemiconductorToday_AprMay2014-GaN-on-silicon.pdf

1.2. Research objective

This thesis aims to study the MOCVD growth of GaN on Si (100) substrate patterned with V-grooves. It is observed that by placing the V-grooves' Si (111) facets perpendicular to precursor flow, single facet growth of GaN is achieved without masking the other facet with silicon oxide or nitride. Simulation study in COMSOL environment will be performed to study the growth mechanisms of GaN on V-groove patterned silicon substrate. The aim is to clarify the impact of V-groove directions to gas flow on the growth mechanism and morphology of GaN. Lastly, this thesis will explore the prospects of cascading light emitting devices based on GaN / InGaN single quantum well in a V-groove, together with fiber in an adjacent bigger V-groove to couple light out for analysis. This could be used for single-photon generation and detection technology.

1.3. Organization of the thesis

Chapter 1 has given an overview of GaN-on-Si technology, with emphasis on selective area growth. Chapter 2 starts with providing a literature review on GaN growth on patterned silicon substrate. Growth of GaN on Si (100) substrate patterned with V-grooves by EMCORE D180 MOCVD is then presented. The GaN quality would be characterized by scanning electron microscopy (SEM) and transmission electron microscopy (TEM). Chapter 3 will first present a review of GaN MOCVD growth simulation. The physics models of COMSOL software will be then be introduced. Then, simulation is performed to study the impact of V-groove directions with respect to precursor flow on the growth mechanism and

morphology of GaN. The results will be compared with and corroborate experiment results in Chapter 2. Chapter 4 will study the prospects of using quantum well intermixing to create a quantum dot region within InGaN / GaN quantum well in a V-groove. The structure is cascaded to a single-mode fiber in an adjacent bigger V-groove to couple light out for analysis. This proposed structure's possible applications for single-photon technology will be discussed. The thesis will end with a summary and recommendations for future work.

Chapter 2 MOCVD growth of GaN on Si (100) substrates patterned with V-grooves

2.1. Overview of GaN growth in MOCVD

The mainstream commercial equipments used for growth of GaN include metalorganic chemical vapor deposition (MOCVD, also known as organo-metallic vapor phase epitaxy or OMVPE) and molecular beam epitaxy (MBE). These two equipments have different advantages and disadvantages. The MBE method does not require carrier gas and could produce crystalline growth with better quality. However, the deposition rate is slow, which is normally less than 1000 nm per hour. (Long & McIntyre, 2012) Thus, it is not suitable for large-scale industrial production.

In comparison, MOCVD usually uses hydrogen or nitrogen as carrier gas, and the deposition rate is higher than MBE, usually in the range of several microns per hour. The MOCVD technology is versatile and economical. It is widely used for large-scale industrial production of light-emitting diodes (LEDs), laser diodes (LD), solar cells, transistors and other optoelectronic devices. Its extensive use in industry also spurs research and development of growing new and better quality materials. In this work, Emcore D180 vertical chamber rotating-disk MOCVD system will be the focus of study.

2.2. MOCVD equipment

In the development history of MOCVD equipments, various types of reactors have been invented, with the aim of providing facilitating growth environment for crystalline materials. The types of reactors include horizontal reactor, vertical reactor and planetary reactor. (Yao & Hong, 2009) In Figure 2-1 below, schematics of various types of MOCVD reactors are illustrated. For horizontal reactor (Figure 2-1 b), the reactant gases are fed in parallel flows to the substrate. In vertical reactor, the precursor flow is injected through nozzles perpendicularly to the substrate.

An important variant of vertical reactor is the rotating-disk vertical reactor (Figure 2-1 a), in which the susceptor rotates at speed over 1000 rpm. The rotating susceptor functions as a centrifugal pumping device, drawing precursors injected from nozzles down to the susceptor, and spread them over the substrate surface in an evenly manner. In such reactors, the inlet nozzles have to be placed in a distance away from the heated susceptor, in order to prevent overheating of the inlets. The planetary reactor is usually a large system. On top of a main rotating susceptor reside multiple smaller sub-susceptors (Figure 2-1 c). While the main susceptor rotates, sub-susceptors will simultaneously rotate around their own axis, in a similar fashion as planets' rotation around the sun while self-rotating. In this thesis, the MOCVD equipment used for GaN growth is EMCORE D180 TurboDisc Vertical Chamber MOCVD. Its dimensions are listed in Table 2-1 below.

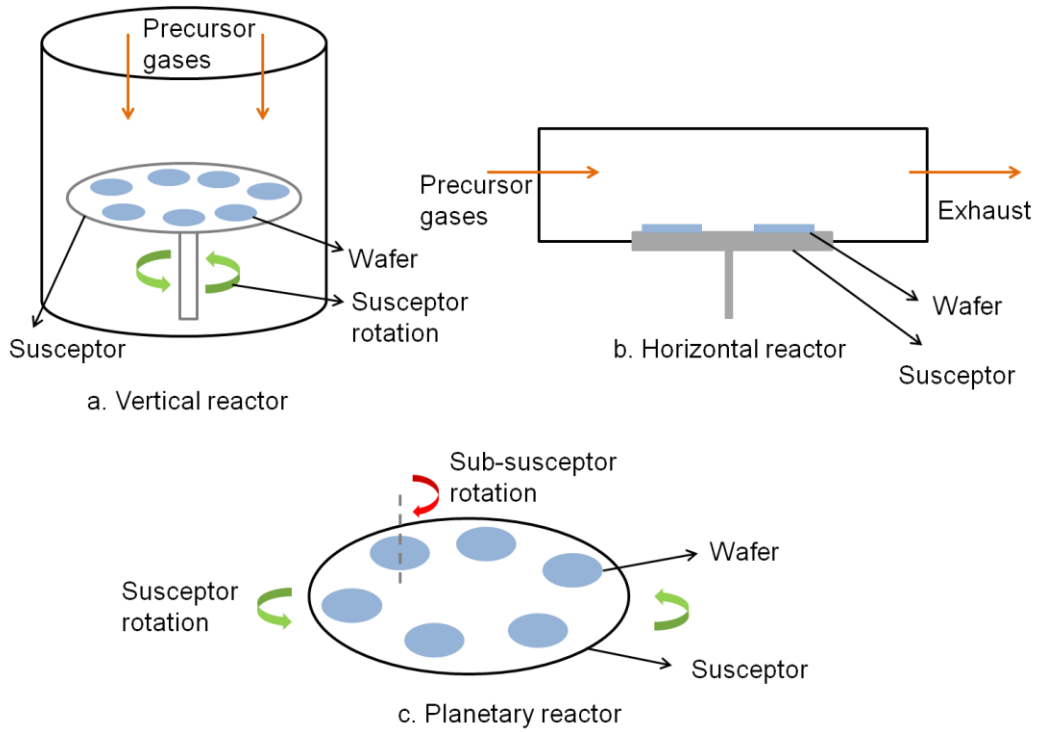


Figure 2-1. Schematics of variants of MOCVD reactors: (a) rotating-disk vertical reactor (b) horizontal reactor (c) planetary reactor. Blue circles and rectangles represent wafers placed on susceptor.

Dimension	Unit	Magnitude
Reactor diameter	mm	250
Disk diameter	mm	182
Disk to inlet spacing	mm	125/200
Deposition area	mm ²	2.66 x 10 ⁴
Capacity / run of 50 mm wafers	n.a	7

Table 2-1. Specifications for Emcore D180 TurboDisc vertical reactor.

2.2.1. Precursors

For the growth of GaN in MOCVD, trimethylgallium (TMG) is widely used as the source for gallium (Ga), due to its relatively high vapor pressure. The TMG molecule consists of one Ga atom attached to three methyl groups. It undergoes decomposition and other reactions to supply Ga atoms for GaN growth. It is also more stable compared to the alternative Ga source - triethylgallium (TEGa). The latter could decompose during storage and trigger undesirable reactions during growth. TMG is highly flammable, and catches fire spontaneously if exposed to air. Thus its storage and handling require careful precautions. For the growth of AlN buffer layer, trimethylaluminum (TMAI) is used as the source for aluminum. The most common source for nitrogen used in MOCVD is ammonia gas (NH_3).

2.2.2. GaN growth process

For growth of GaN on sapphire, a standard two-step process is used, as illustrated in Figure 2-2 below. Initially, a pre-nitridation process is performed. Then, a GaN nucleation layer with approximate thickness of 25 nm is grown at a temperature in the range of 520°C to 530°C. This lower-temperature GaN nucleation layer mainly consists of cubic GaN grains. Afterwards, the temperature is increased to 1015°C to 1030°C for GaN growth.

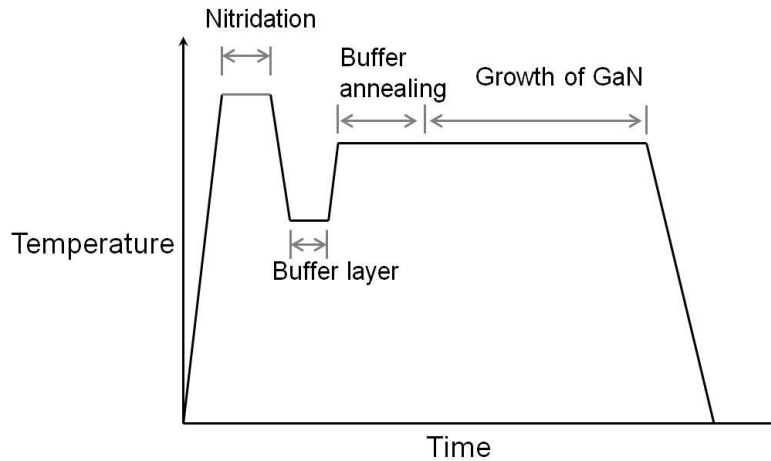
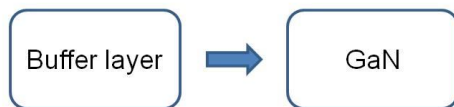


Figure 2-2. Two-step growth flow of GaN on sapphire.

For growth of GaN on silicon, the growth process is more complicated, and includes more growth stages. In Figure 2-3, major stages for growth of GaN on sapphire and silicon substrates are summarized. A major difference is the requirement of an additional intermediate layer for growth on silicon.

(a) Process flow for GaN growth on sapphire



(b) Process flow for GaN growth on silicon

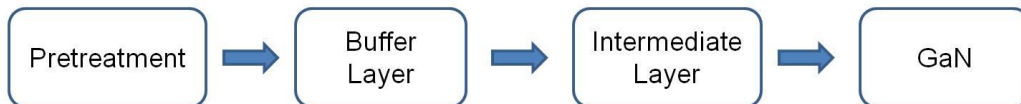


Figure 2-3. Comparison of growth processes for GaN on (a) sapphire and (b) silicon.

As stated in Chapter 1, the most challenging task for growing GaN on Si is to overcome the difference in crystalline structures, vast mismatch in lattice

constants and thermal expansion coefficients between the two materials. The use of an intermediate layer such as AlN causes the nature of strain between GaN and Si to switch from tensile to compressive. Another function of the intermediate layer is to prevent the problem of destructive interactions between Si and GaN. The thermal stability of lower-temperature GaN on Si is much inferior to that on sapphire substrate. (Ishikawa *et al.*, 1998) If the same lower temperature (530°C) GaN buffer layer is used for GaN-on-Si growth, GaN will undergo reactions with out-gassing silicon during thermal annealing at temperature of 1050°C. One type of such reactions is that silicon and gallium atoms could form a eutectic alloy, with melting point as low as 29°C. (Olesinski *et al.*, 1985) These reactions would cause serious etching and damage to GaN grown and lead to the formation of hollow swellings and pits within it, also called the melt-back etching of silicon by gallium. An intermediate layer in between GaN and silicon substrate could shield GaN from reactions with silicon.

The growth of the intermediate layer needs to be carefully designed to ensure good quality. When AlN is used as the buffer layer, the silicon surface could be exposed to an initial short wash of TMAH for 12 seconds, leaving a few monolayers of aluminum atoms on the silicon substrate surface. This step is found to induce good quality GaN layer. (Zhang *et al.*, 2005) After growing the AlN intermediate layer, in order to further reduce the stress between AlN intermediate layer and silicon substrate, multilayer AlN / GaN superlattice could be grown. (Lin *et al.*, 2007) One thing to note is that in this work, the growth of GaN is

performed within V-grooves on silicon substrate, which are limited in size. Thus, the growth stack in this work includes only a 100 nm AlGa_N layer on top of the AlN intermediate layer.

2.3. Overview of GaN growth on patterned silicon substrate

2.3.1. Processing steps

When silicon substrate is used for GaN growth, certain special preparations need to be performed. The dangling bonds on the silicon surface need to be hydrogenated. (Cartier *et al.*, 1993) This is done by immersing the silicon substrate in a 60°C 1:1:1.5 solution of HCl : H₂O₂ : H₂O for 10 minutes. (Morkoç 2009) This would form a porous oxide on the substrate. After washing with deionized water, the silicon substrate is placed in a 10:1 aqueous HF solution for 20 seconds. The exposure to HF would hydrogenate dangling bonds on the silicon surface.

The most matching silicon plane for GaN growth is the Si (111) plane. For silicon substrates with various crystalline orientations other than Si (111), Si (111) facets need to be exposed preceding the growth of GaN. In order to achieve this, the common method used is that a layer of silicon nitride mask is first deposited on the silicon substrate. Standard photolithography process is used to open rectangular strip patterns on nitride mask, in a calculated direction. Then, etching is performed to expose the desired Si (111) facets. The etching could be isotropic dry etching or anisotropic wet etching, depending on the crystalline orientation of

substrate. For wet etching, choices for etchants include tetra methyl ammonium hydroxide (TMAH) and aqueous potassium hydroxide (KOH). Wet etching is anisotropic on silicon, due to different packing factors on different silicon planes. Planes with higher packing factor such as the Si (111) plane would undergo slower etching than planes with lower packing factor.

In most cases, etching on silicon would result in two opposite facets both suitable for GaN growth. For example, in the case of KOH etching of Si (100) substrate, anisotropic etching by KOH will produce a V-shaped groove, with two opposite facets being Si (111) and Si (-1-11) planes. In order to achieve epitaxial lateral overgrowth (ELO), one facet has to be masked with silicon oxide, in order to prevent simultaneous growth from the two opposite facets and subsequent meeting of the two GaN crystals, which could result in defects or even collapse of the crystal grown. The equipment used for this purpose is the Glancing Angle Deposition Stage (GLAD), as illustrated in Figure 2-4 below. It is a modified version of electron beam deposition (EBL). The substrate is mounted on a rotation motor capable of two axis rotations. By rotating the substrate, one can selectively deposit materials on desired parts of the substrate. In the case of growing GaN on patterned silicon substrate, GLAD is utilized to deposit silicon dioxide on one of the matching facets for GaN growth. In the case of Si (100) substrate patterned with V-grooves, either Si (111) plane or Si (-1-11) plane could be masked. Masking one facet by GLAD could help prevent simultaneous growth on two facets, but it requires extra equipment and processing step. In Section 2.4 below,

an observation is reported that, by placing V-grooves on Si (100) substrate perpendicular to the direction of precursor flow on susceptor, single-facet growth is achieved without masking either of the V-groove facets.

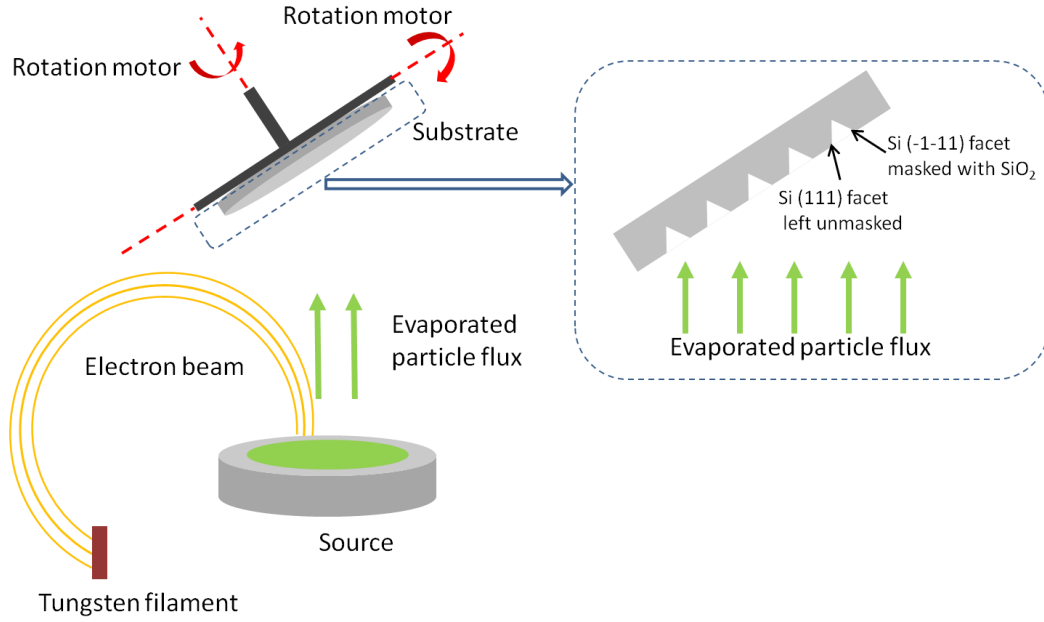


Figure 2-4. Schematic of Glancing Angle Deposition system (GLAD).

2.3.2. Growth of GaN on silicon substrates with various crystalline orientations

A technical advantage provided by GaN-on-Si technology is that, it is relatively easy to produce different planes of GaN by performing growth of it on silicon substrates with various crystalline orientations. For example, semi-polar GaN (1-101) could be obtained by growth on Si (100) substrate, and non-polar GaN (11-20) could be obtained by growth on Si (110) substrate. Below, a brief review of polarization effect in GaN is presented, and a number of combinations between Si substrate and GaN are reviewed.

The thermodynamically stable structure of GaN is wurtzite, with hexagonal unit cells. GaN exhibits significant polarization effect, including both spontaneous polarization and piezoelectric polarization. Polarization effect in GaN induces a significant built-in internal electric field. Under the influence of this built-in electric field, energy band would tilt in active region, thus causing electrons and holes to separate. The overlap of electron and hole wavefunctions will be reduced. For strained InGaN / GaN quantum wells, the transition energy will be reduced, as the band alignment of well is tilted by the piezoelectric field. Such effect is called the quantum confined stark effect (QCSE). Photogenerated carriers under excitation would screen the piezoelectric field. (Takeuchi *et al.*, 1997) This screening effect is more pronounced for high indium content quantum wells, and it is believed to be hindering the realization of high efficiency LEDs or laser diodes in the green light region.

The root cause of the above mentioned problems is that GaN is usually grown in polar (0001) axis. A logical solution is to utilize semi-polar and non-polar planes of GaN, in which the effective polarization is given by the projection of polarization vector to growth direction. (Romanov *et al.*, 2006) In order to achieve growth of semi-polar or non-polar GaN, homoepitaxy on native substrate with matching crystalline orientation could be used, but native GaN substrates have issues of limited availability and high cost.

In this backdrop, silicon substrates are an attractive alternative, and could be used for semi-polar and non-polar GaN growth. One advantage offered by using silicon substrate for GaN growth is that, silicon substrates are readily available in different crystalline orientations, as shown in Figure 2-5.

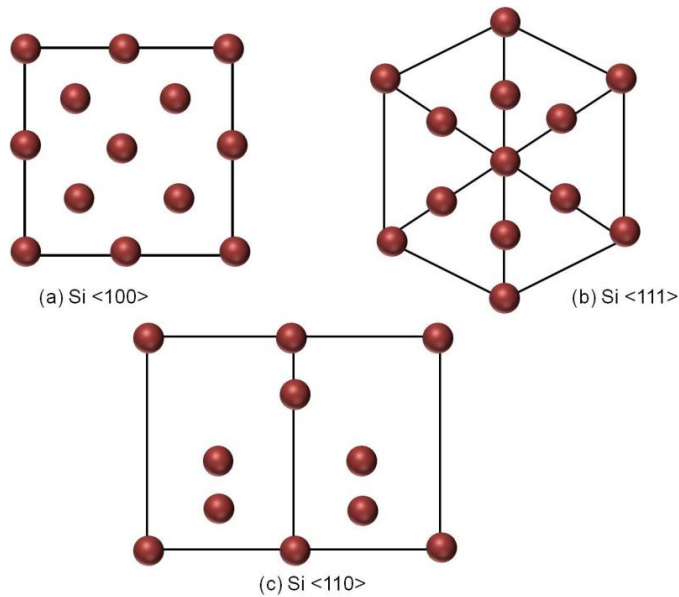


Figure 2-5. Silicon atomic structure as viewed from different crystalline directions.

By forming Si (111) facets on various substrates, GaN in different crystalline orientations (Figure 2-6) could be obtained. This offers a convenient method to obtain semi-polar or non-polar GaN planes for further device fabrication. A number of combinations between silicon and GaN with matching crystalline orientations will be reviewed: GaN (1-101) on Si (001), GaN (11-22) on Si (113), GaN (11-20) on Si (110), and GaN (1-100) on Si (112).

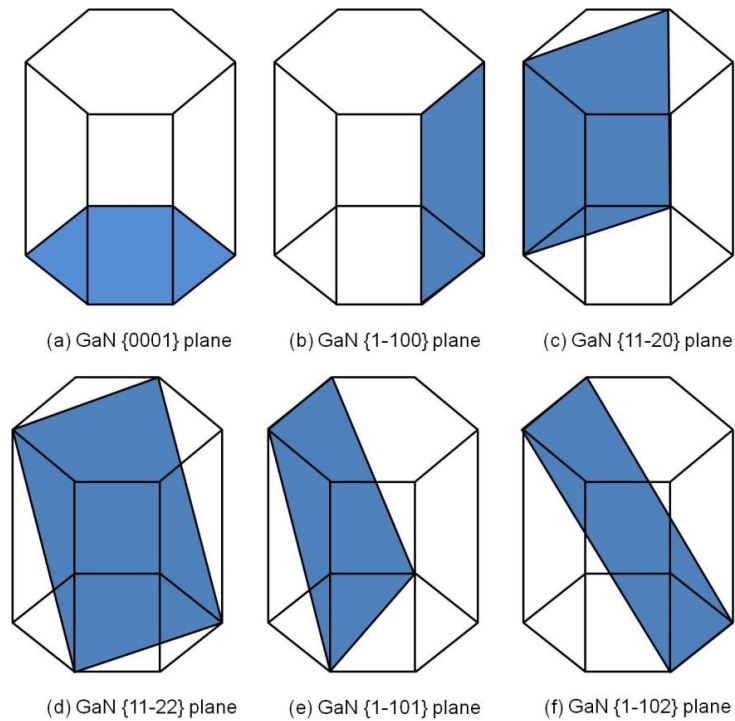


Figure 2-6. Various planes in GaN unit cell.

(a) Growth of GaN (1-101) on Si (100) substrate

The current industrial standard for substrate of CMOS-based integrated circuit is Si (100) substrate. Achieving growth of GaN on Si (100) substrate is particularly crucial, as it is the key to integration of GaN-based devices with silicon-based electronics. However, Si (100) is not the most suitable silicon platform for the growth of GaN. This is because the Si (100) plane has a larger lattice mismatch to GaN, compared to Si (111) substrate. Also Si (111) substrate's trigonal crystal symmetry favors more the growth of GaN (0001) plane. A way to solve this dilemma is to expose Si (111) facets on Si (001) substrate by anisotropic etching.

The process flow of growing GaN on patterned Si (100) substrate is illustrated in Figure 2-7 below. (Sawaki *et al.*, 2009) A trapezoidal trench with flat bottom is first formed on a 7.3° off-oriented Si (001) substrate, through anisotropic etching by KOH. Si (111) and Si (-1-11) facets are exposed as a result. Si (-1-11) facet is then masked by silicon oxide, before the substrate is loaded into MOCVD chamber for GaN growth. A 7.3° off-oriented Si (001) substrate is used instead of a nominally-cut one. This is because the lateral overgrowth of GaN from Si (111) facet of a 7.3° off-cut substrate would result in a planar and horizontal top semi-polar GaN (1-101) surface, instead of a tilted surface for the case of nominally-cut substrate. The planar top semi-polar GaN (1-101) plane could then be conveniently used as a platform for fabrication of devices such as light emitting diodes.

As illustrated in Figure 2-7, GaN growth would initiate from the Si (111) facet, which has a 50-nm AlN intermediate layer grown on it. When GaN grown extends out of the groove, it would extend laterally over the mask and grow in the [1-101] direction as well. As a result of coalescence between laterally-grown GaN and some GaN grains deposited on SiO₂ mask, stacking faults are observed. (Sawaki *et al.*, 2009) To study the crystal quality of GaN (1-101) grown, high resolution transmission electron microscopy (TEM) is used in the literature. It is found that threading dislocations at the interface between silicon and GaN would bend to the horizontal direction, leaving fewer dislocations propagating in the vertical direction. (Tanaka *et al.*, 2002) Thus, the top semi-polar surface of (1-101)

GaN has a better quality for device fabrication.

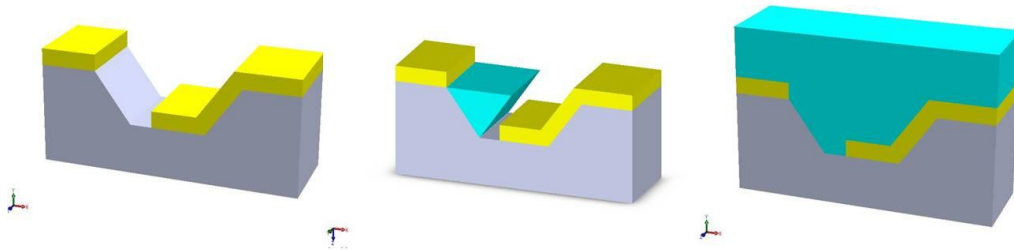


Figure 2-7. Process flow for growth of GaN on 7° off-cut Si (100) substrate.

One thing to note is that, for growth of GaN on Si (100) substrate in this thesis, a nominally-cut Si (100) is used. V-shaped grooves are formed instead of trapezoid trenches.

(b) Growth of GaN (11-22) on Si (113) substrate

For growth of GaN on Si (113) substrate, photolithography is first used to open strip patterns on nitride mask along the $\langle 21-1 \rangle$ direction. Then, etching will expose the Si (111) facets, which are at an angle of 58.5° to the (113) plane. In this case, masking one facet is not required. It is because the right-side Si (111) facet is inclined inwards and would not receive sufficient precursors from inlets above for growth. Also, there will not be substantial growth of GaN on the bottom surface of the trench, because it would not receive sufficient amount of precursor injected from inlets above. The final top surface grown is a semi-polar GaN (11-22) surface.

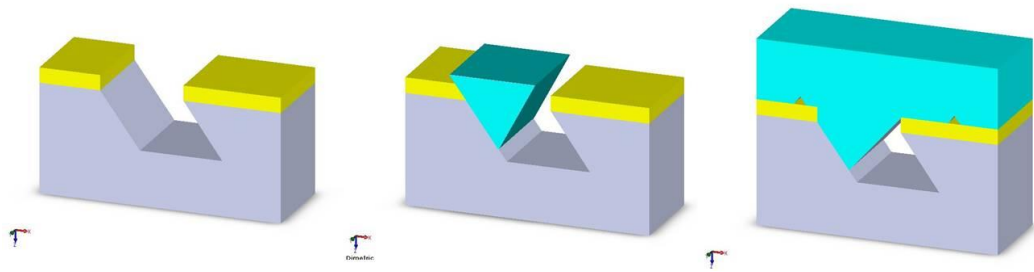


Figure 2-8. Process flow for growth of GaN on Si (113) substrate.

(c) Growth of GaN (11-20) on Si (110)

For growth of GaN on Si (110) substrate, Si (111) planes formed by etching are perpendicular to the substrate. One facet of the rectangular trench is masked by SiO₂. The top surface grown is GaN (11-20), which is non-polar. The c-axis of GaN in this case is parallel to substrate surface. (Tanikawa *et al.*, 2008)

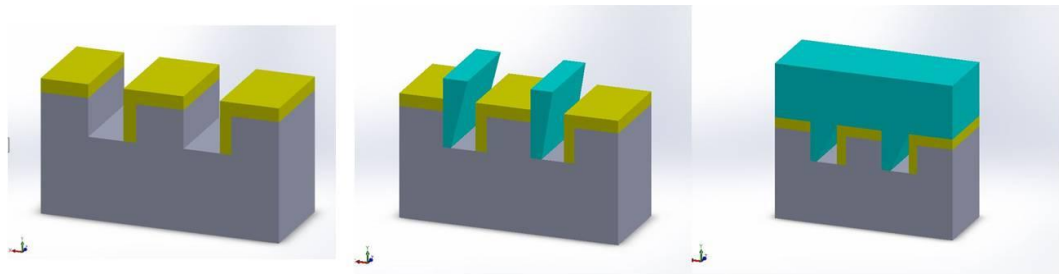


Figure 2-9. Process flow for growth of GaN on Si (110) substrate.

(d) Growth of (1-100) GaN on Si (112)

For growth of GaN on Si (112) substrate, strip patterns are opened on nitride mask in the Si (1-10) direction. After etching, the Si (-1-11) plane is perpendicular to the substrate, and growth would initiate from this plane. The c-

axis is parallel to the substrate, and threading dislocations would not propagate to the top surface. The top surface is GaN (1-100) plane. (Ni *et al.*, 2010)

2.4. Growth of GaN in EMCORE D180 MOCVD

2.4.1. Growth equipment

The MOCVD equipment used in this work is Emcore D180 TurboDisc vertical reactor. This section of work is performed in collaboration with Dr. Kwadwo Konadu Ansah-Antwi, and has resulted in a manuscript in preparation for submission to journal, as listed in the publication list in appendix. The gas inlets consist of one hydride zone for injection of ammonia and two alkyl zones for injection of TMG. The designated gas delivery passages for hydride and alkyl species are spaced at a distance from each other. This is to prevent premature contact among reactants and subsequent reactions, which would disturb chamber reactions.

2.4.2. Substrate preparation

The silicon (100) substrate preparation starts with surface cleaning by immersing the substrate in acetone for ten minutes. It is then cleaned with isopropanol alcohol (IPA). Afterwards, degreasing process is carried out by immersing the substrate in piranha solution at 120°C. The piranha solution is a mixture of H₂SO₄ and H₂O₂, with 3:1 ratio between concentrated sulfuric acid and 30% hydrogen peroxide solution. A strong oxidizing agent, piranha solution could help remove

organic contaminants on the substrate surface. One thing to note is that great care should be paid for the preparation of piranha solution. The mixing procedure should be performed by adding H_2O_2 to H_2SO_4 acid, and not in the reverse sequence. The mixing process is highly exothermic, and it has to be gradually performed to prevent boiling the solution and releasing corrosive fumes. Then, in order to remove the native oxide on the silicon substrate, the substrate is placed in a 7:1 buffered hydrofluoric acid solution for a short period of time.

2.4.3. Substrate patterning

The processing steps for Si (100) substrate patterning are shown in Figure 10 (a). The cleaned silicon substrate is then loaded into the chamber of a plasma enhanced chemical vapor deposition system (PECVD), to deposit a 100 nm thick silicon nitride mask layer.

The Si (100) substrate used has its primary flat cut in the $\langle 110 \rangle$ direction. Standard photolithography process is used to pattern rectangular window openings on the nitride mask along the $\langle 110 \rangle$ direction, with the dimensions of 4 μm in width and 100 μm in length. Then, the substrate is immersed in an aqueous potassium hydroxide (KOH) solution for wet etching, in order to expose the Si (111) facets. The etching solution is 45% by weight aqueous KOH solution mixed with 15% (v/v) isopropyl alcohol (IPA). The etching solution is heated to 75°C and the etching time is 10 minutes.

The etching process will produce V-groove trenches on the Si (100) substrate, having width of 4 μm , depth of 2.82 μm , and separated by 4 μm silicon nitride mask. The SEM image is shown in Figure 2-10 (b). The angle of tilt for Si (111) facet with respect to horizontal is 54.7° .

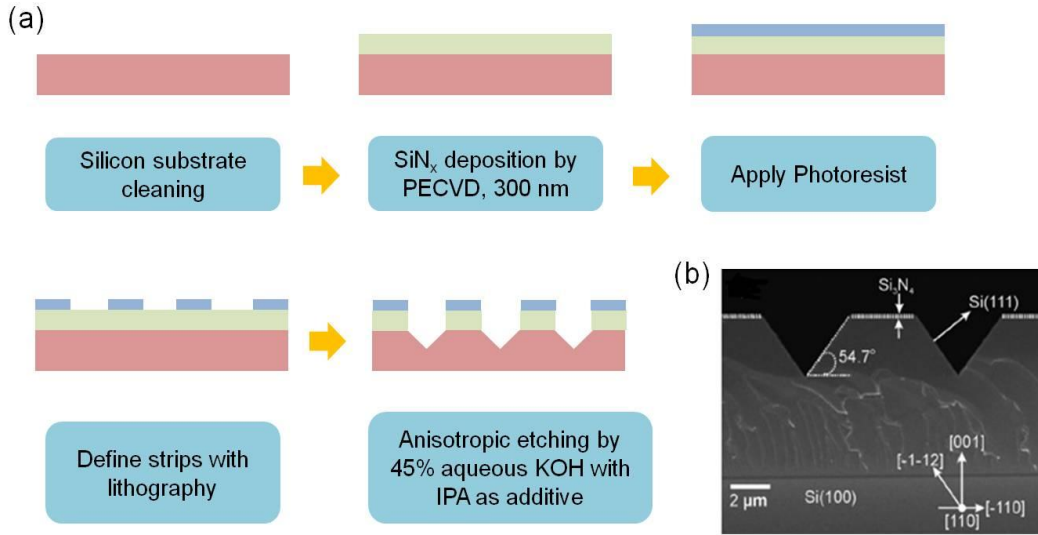


Figure 2-10. Schematic illustrating the processing steps for patterning V-grooves on Si (100) substrate for GaN growth.

2.4.4. MOCVD growth of GaN

In this section, MOCVD growth of GaN is performed on Si (100) substrate patterned with V-grooves. The aim is to investigate the impact of V-grooves placement directions relative to precursor flow within the reactor chamber on GaN growth mechanisms and resulting morphology. Three Si (100) substrates patterned with V-grooves are prepared and labeled as Sample A, B and C. The longitudinal axis of V-grooves of different samples are placed at specific angles with respect to radial direction of susceptor, which coincides with the precursor flow direction. As illustrated in Figure 2-11 below, for Sample A, V-grooves are

placed at 0° to radial direction; for Sample B, V-grooves are placed at 45° to radial direction; for Sample C, V-grooves are placed at 90° to radial direction. The precursor flow direction is indicated by the red arrow.

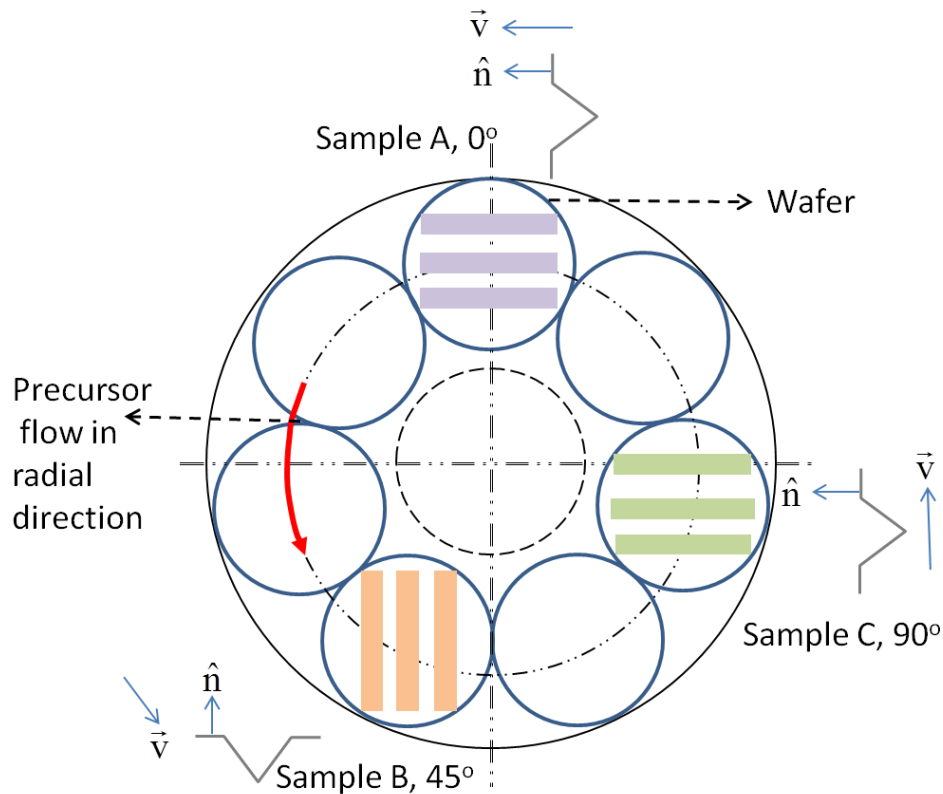


Figure 2-11. Layout of susceptor loaded with V-groove-patterned Si (100) substrates, with V-grooves aligning in 0° , 45° , 90° to precursor flow (red arrow) for Samples A (purple grooves), B (orange grooves) and C (green grooves) respectively. \vec{v} denotes the direction of precursor flow. \hat{n} denotes the normal direction to V-grooves.

The sources used for gallium, nitrogen and aluminum are trimethylgallium (TMGa), ammonia (NH₃) and trimethylaluminum (TMAI) respectively. The precursors are diluted in hydrogen carrier gas.

Prior to growth, substrates are cleaned in 10% aqueous hydrofluoric acid, in order to remove the easily formed silicon oxide layer on the substrate surface. After placing the substrates on susceptor, the chamber is sealed for deposition. The growth stages are as follows. Firstly, an AlN buffer layer of 50 nm is grown, at pressure of 80 Torr, temperature of 1020°C, and V/III ratio $R_{V/III} = 1000$. Then a 100 nm layer of $Al_{0.3}Ga_{0.7}N$ is grown to help absorb and withstand the stress induced between GaN and silicon substrate, and prevent cracking especially during the cooling stage. Finally, the GaN layer growth is performed with pressure of 90 Torr, temperature of 1010°C, and $R_{V/III}=2000$. The stack of layers grown on Si (111) facets are illustrated in Figure 2-12.

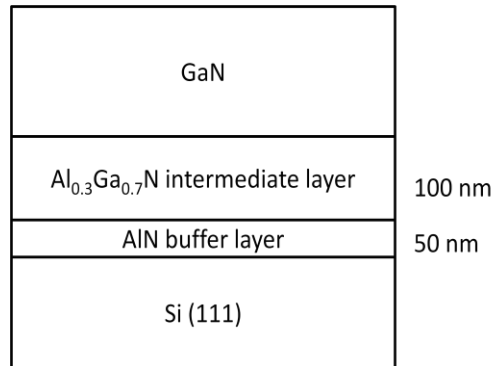


Figure 2-12. Schematic illustrating the stack of material layers grown on Si (111) facets of V-grooves patterned on Si (100) substrates.

2.4.5. characterization

The growth morphology of GaN obtained is characterized by a JEOL 6700F field-emission scanning electron microscope (FE-SEM) system. For Sample A, having V-grooves at 0° to radial direction, i.e. parallel to precursor flow, there is no significant visible growth of GaN within the trenches, as shown in Figure 2-13(a).

For Sample B, having V-grooves at 45° to radial direction or precursor flow, there is one smaller and one larger triangular prisms on opposite facets of V-grooves respectively, as highlighted in red in Figure 2-13(b). For Sample C, having V-grooves at 90° to precursor flow direction, i.e. perpendicular to precursor flow, GaN grown exhibits single-facet growth, as highlighted in red in Figure 2-13(c).

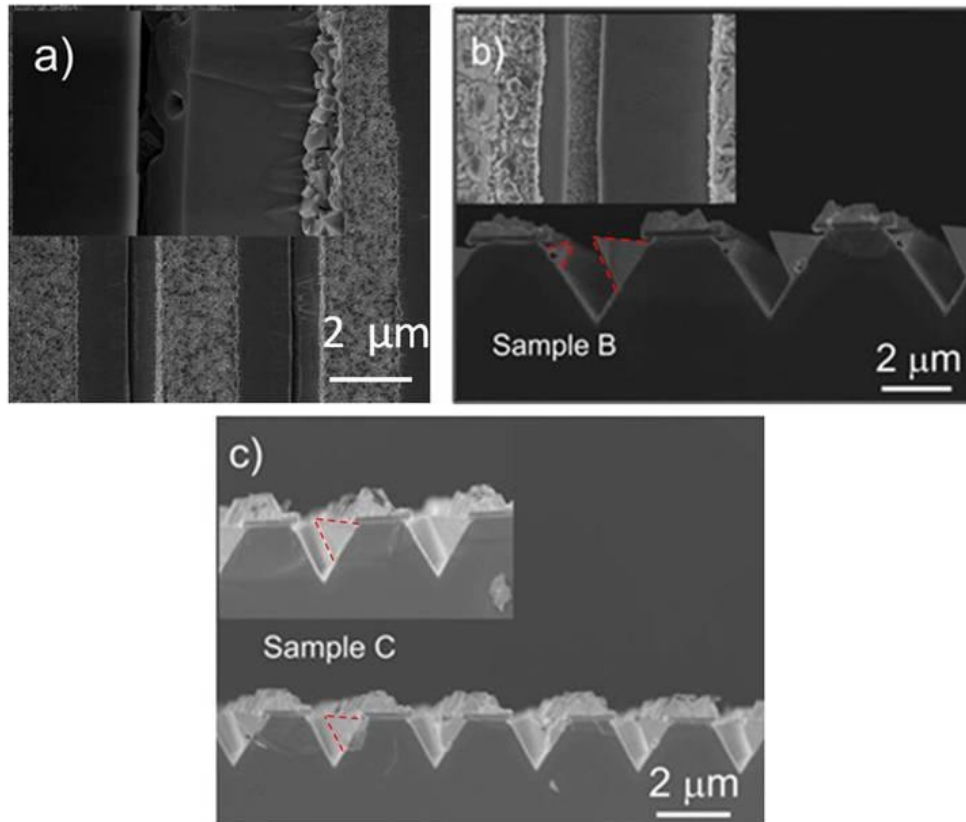


Figure 2-13. SEM images of (a) Sample A (b) Sample B (c) Sample C.

In Figure 2-13, the materials with non-uniform thickness grown on top of the nitride mask are GaN poly-crystals. This kind of undesirable growth would happen when the growth temperature and pressure are not optimal. With optimal growth conditions, there will not GaN poly-crystals deposited on the mask, and growth of GaN would only take place on the V-groove facets, as illustrated in

Figure 2-14. Figure 2-14 is a depiction of GaN grown for sample C, when the growth time is increased to 20 minutes. It can be seen that there is no undesirable growth of GaN poly-crystals on the mask, and the top (1-101) surface of GaN is smooth with no observable defects and pits.

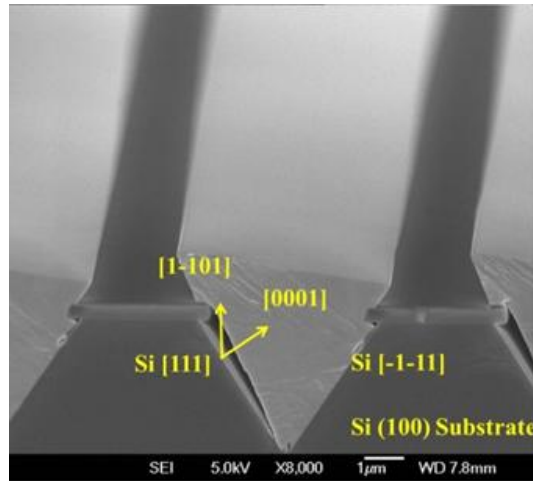


Figure 2-14. SEM image of Sample C after a growth time of 20 minutes.

The quality of the GaN grown in Sample C is studied by photoluminescence spectroscopy (PL). PL is chosen as the main characterization technique, because the ultimate aim of the GaN growth in this work is for fabrication of optical devices. TEM and XRD are not employed due to the small dimension of the structure grown. The PL spectra is shown in Figure 2-15 below. The full width at half maximum (FWHM) is approximately 30 nm. The absence of yellow band indicates the low level of defects in GaN crystal.

From experiments above, it is observed in Sample C that, without masking one facet of V-grooves on Si (100) substrate, by placing the V-grooves perpendicular to precursor flow direction, single-facet growth of GaN is achieved. This

observation is corroborated by two other samples A and B. When the V-grooves are aligned at an angle of 45° to the precursor flow in Sample B, growth takes place on both facets, whereas one triangular prism grown is bigger than the other. When the V-grooves are aligned in parallel to radial precursor flow direction in Sample A, no observable growth takes place on either of the V-groove facets.

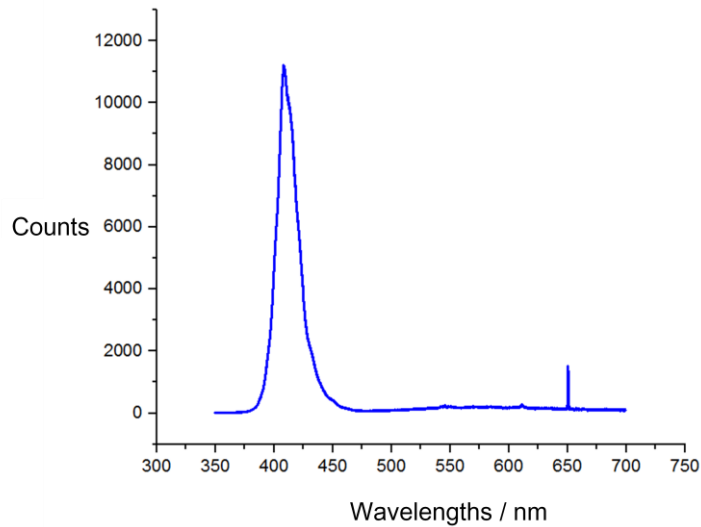


Figure 2-15. PL spectra of GaN grown in Sample C.

A trend could be extrapolated that a possible relationship exists between the relative direction of surface V-groove with respect to precursor flow, and GaN growth morphology on Si (100) substrates patterned with V-grooves. In terms of practical application, this observation could be utilized to replace the masking step in epitaxial lateral overgrowth of GaN on silicon, and thus simplify the process flow and save cost of equipment. In order to understand this observation, simulation of GaN growth mechanisms on Si (100) substrate patterned with V-

grooves is performed in COMSOL software, and the results are presented in Chapter 3.

Chapter 3 Simulation of GaN growth on Si (100) substrates patterned with V-grooves

3.1. Motivation for MOCVD simulation

Simulation of material growth in MOCVD has received great attention from the research and industry communities, due to its enormous economic and efficiency benefits. The cost per run of MOCVD is expensive. The issue of high cost per run is aggravated by the trend that MOCVD chambers are increasing in size to accommodate more wafers, in order to achieve economies of scale in the industry. In this backdrop, simulation provides a way to better design experiments, by optimizing reaction parameters beforehand and reduce the number of trial runs. Moreover, simulation could yield in a more thorough analysis and understanding of the growth results, and facilitate the improvement of growth processes. For MOCVD equipment manufacturers, simulation of reaction kinetics and dynamics within the reactor chamber could help investigate and verify new designs, and yield in better understanding and proper design of the chamber. In the field of scientific research, MOCVD is increasingly used for the growth of III-V materials on silicon platforms to achieve their integration and improve the performance of devices such as MOSFETs and HEMTs. MOCVD simulation could help us understand the growth issues arising from the integration of two different material systems, and find solutions for improving the material quality.

In this thesis, in order to investigate and understand the growth mechanisms of GaN on V-groove-patterned Si (100) substrates, simulation is performed in the COMSOL[®] software. Particularly, the simulation is aimed at investigating and explaining the observation in Chapter 2, that single-facet growth of GaN is achieved when V-grooves on Si (100) substrate are placed perpendicular to the direction of precursor flow.

In order to achieve the above mentioned goals, the approach for simulation of GaN growth should be carefully selected, as there are several simulation methods focusing on different aspects of GaN growth. One approach is Computation Fluid Dynamics (CFD) simulation, which studies the flow and distribution of precursors within the reactor by computing the distributions of velocity and temperature. Another approach is the study of atomic assembly using various methods such as molecular dynamics (MD) simulation, which simulates the mechanism of atomic deposition during GaN growth. (Zhou *et al.*, 2006) In this work, CFD simulation is chosen to be the simulation approach. This is because the aim of this work is to study the impact of silicon substrate's V-grooves on the growth dynamics of GaN. The presence of V-grooves are likely to have an effect on the distribution of precursors on the substrates. Although CFD simulation does not directly simulate actual growth morphology of GaN, it could provide us with crucial information such as precursor velocity and pressure for prediction of GaN growth. To achieve this, the partial pressures and atomic masses of the precursors would be taken into

account, and precursor flow supplying the atomic constituents for GaN growth would be the focus of study. Furthermore, parameters like precursor velocity and reactor temperature could be used to construct the simulation model for simulation of atomic assembly. The result in this thesis could serve for future work on simulation of atomic assembly and study of deposition mechanisms and morphology.

The MOCVD simulation in this thesis is a two-step process. The first step is to feed reactions leading to GaN growth into the space-independent “Chemistry” interface of COMSOL, in order to compute important parameters of the batch reactor. In the second step, a space-dependent study based on real dimensions of the MOCVD reactor is set up, and the Laminar Flow and Heat Transfer modules in COMSOL will be utilized to compute the distributions of velocity, pressure and temperature within the MOCVD reactor chamber. A comparison would be made between flat substrates and substrates patterned with V-grooves, in order to investigate the impact of V-grooves on the growth mechanisms and dynamics of GaN.

The two-step simulation process above requires an understanding of the growth reactions leading to GaN growth, as well as MOCVD reactor chamber design principles and growth dynamics within. Therefore, in the following sections, a review will be first presented for reactions leading to GaN growth in MOCVD,

followed by a review for MOCVD reactor design. Then, the simulation setup and results in COMSOL will be presented.

3.2. Review of MOCVD growth of GaN

3.2.1. Reactions leading to growth of GaN

Due to the intrinsic complexity of chemical reactions leading to growth of GaN in MOCVD, there is yet to be an unambiguous consensus on the growth processes and mechanisms. The main differences and ambiguities reside in intermediate reactions, the relative importance of gas-phase reactions' role in determining deposition kinetics (Chen *et al.*, 1995; Pawlowski *et al.*, 2000), and values of reaction rate parameters such as activation energies and reaction rate constants.

Despite discrepancies in the exact sequence of reactions leading to the growth of GaN in MOCVD, there is a consensus on a number of major gas-phase and surface chemical reactions. When gas-phase precursors (trimethylgallium (TMG) and ammonia) are injected into the growth chamber, gas-phase chemical reactions would take place first. These reactions could be classified into two competing routes: one is adduct formation pathway, and the other is thermal decomposition of TMG pathway, as illustrated in Figure 3-1 below. For adduct formation, the starting point is the interaction between TMG and ammonia, which will result in the formation of stable Lewis acid – Lewis base adducts. (Almond *et al.*, 1992) The formed adducts would then undergo intermediate decompositions and

interactions to form GaN and methane (CH₄), as shown in the upper box of Figure 3-1. On the other hand, the TMG thermal decomposition route shown in the lower box of Figure 3-1 would result in Ga atoms and a methyl group, which would take part in surface reactions and form GaN.

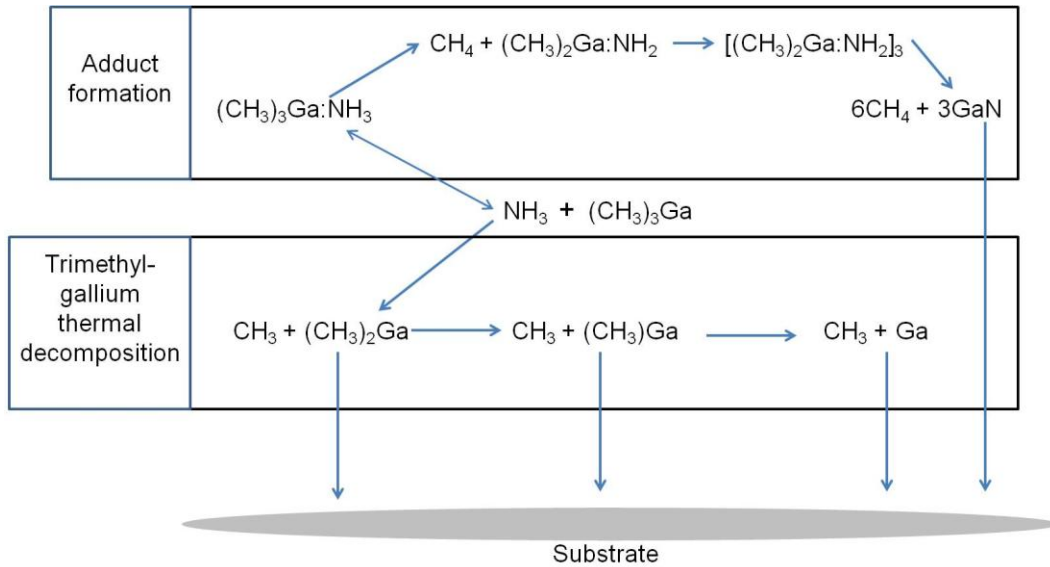


Figure 3-1. Gas-phase reaction pathways for GaN growth in MOCVD. Adapted from (Parikh & Adomaitis, 2006)

In Tables 3-1 to 3-3 below, major gas-phase and surface reactions leading to growth of GaN are listed, based on a review by Parikh et al. (Parikh & Adomaitis, 2006) These reactions would be used in Section 3.3 to model the precursors in batch reactor.

(i) Gas-phase reactions

In Table 3-1 below, gas-phase reactions involving thermal decomposition of TMG are presented. In Equations 1-3, TMG decomposes in three stages to

generate Ga atoms, while expelling one methyl radical (CH_3) in each stage. Equations 4-6 capture the formation of methane (CH_4) and ethane (C_2H_6) as by-products. According to a report by Thon et al., the thermal decomposition process of TMG will be triggered when the temperature exceeds around 723 K. (Thon & Kuech, 1996) This would set a minimum temperature requirement for the growth of GaN in MOCVD.

The commonly used nitrogen source for GaN growth is ammonia. It undergoes a pyrolysis pathway to generate nitrogen atoms. Various studies have indicated that the extent of decomposition of NH_3 would be limited, especially when the temperature is below 1073K. (Monnery *et al.*, 2001) In order to compensate for the low decomposition rate of ammonia, high growth temperature and high V/III ratio are used. (Lobanova *et al.*, 2006). This could facilitate the thermal decomposition of ammonia into active nitrogen species (N , NH , NH_2), and supply enough nitrogen atoms for the growth of high quality GaN epitaxial films. Although ammonia has the disadvantage of low decomposition rate under low temperature and being corrosive, it is still widely used. This is because other alternatives of nitrogen source, such as hydrazine or hydrogen azide, are toxic and flammable. In comparison, ammonia is much safer to handle with.

	Thermal decomposition of TMG
1	$(\text{CH}_3)_3\text{Ga} \rightarrow (\text{CH}_3)_2\text{Ga} + \text{CH}_3$
2	$(\text{CH}_3)_2\text{Ga} \rightarrow (\text{CH}_3)\text{Ga} + \text{CH}_3$
3	$(\text{CH}_3)\text{Ga} \rightarrow \text{Ga} + \text{CH}_3$
4	$\text{CH}_3 + \text{H}_2 \rightarrow \text{CH}_4 + \text{H}$
5	$\text{CH}_3 + \text{CH}_3 \rightarrow \text{C}_2\text{H}_6$
6	$\text{CH}_3 + \text{H} \rightarrow \text{CH}_4$

Table 3-1. Gas phase reactions of GaN growth involving decomposition of TMG.

Table 3-2 lists gas-phase reactions involving adducts formation and oligomerization, as the result of important interactions between TMG and ammonia. In Equation 1, TMG accepts an electron pair from NH_3 , and thus forming a Lewis acid-Lewis base adduct $(\text{CH}_3)_3\text{Ga} : \text{NH}_3$. This is because TMG is electron deficient with the Ga atom having an empty p-orbital. The reaction in Equation 1 represents the initial stage of coordination between group III and group V sources, and is believed to have a significant effect on following reactions. Equation 2 is its reverse reaction. In Equations 3-4, the adduct formed eliminates methane molecules. In Equation 5, three molecules of $(\text{CH}_3)_2\text{Ga} : \text{NH}_2$ combine to form a trimer $[(\text{CH}_3)_2\text{Ga} : \text{NH}_2]_3$. In the final step, the dissociation of the trimer leads to GaN and CH_4 .

	Adduct formation and oligomerization
1	$(\text{CH}_3)_3\text{Ga} + \text{NH}_3 \rightarrow (\text{CH}_3)_3\text{Ga} : \text{NH}_3$
2	$(\text{CH}_3)_3\text{Ga} : \text{NH}_3 \rightarrow (\text{CH}_3)_3\text{Ga} + \text{NH}_3$
3	$(\text{CH}_3)_3\text{Ga} : \text{NH}_3 \rightarrow (\text{CH}_3)_2\text{Ga} : \text{NH}_2 + \text{CH}_4$
4	$(\text{CH}_3)_3\text{Ga} : \text{NH}_3 + \text{NH}_3 \rightarrow (\text{CH}_3)_2\text{Ga} : \text{NH}_2 + \text{NH}_3 + \text{CH}_4$
5	$3[(\text{CH}_3)_2\text{Ga} : \text{NH}_2] \rightarrow [(\text{CH}_3)_2\text{Ga} : \text{NH}_2]_3$
6	$[(\text{CH}_3)_2\text{Ga} : \text{NH}_2]_3 \rightarrow 3\text{GaN} + 6\text{CH}_4$

Table 3-2. Gas phase reactions of GaN growth involving adduct formation and oligomerization.

(ii) Surface reactions

Growth of GaN on the substrate surface involves a number of stages, including adsorption of reactants onto the substrate surface, and movement of atoms into active sites for combination and growth. In Table 3-3 below, surface reactions leading to GaN growth is summarized. The letter “S” denotes active sites on the substrate. Moreover, due to the commonly used high V/III ratio for GaN growth, it is assumed that reactions on the substrate surface are limited by the amount of gallium-containing species arriving on growth sites available on substrate, rather than the arrival rate of nitrogen-containing species.

Equations 1-4 denote the arrival of TMG on substrate surface and decomposition into gallium atoms. In Equations 5-6, adducts of $(\text{CH}_3)_3\text{Ga} : \text{NH}_3$ and $(\text{CH}_3)_2\text{Ga} : \text{NH}_2$ arrive at active sites on substrate surface, forming GaN and eliminating

methane molecules. Equation 7 and 8 depict the deposition of GaN by the trimer $[(\text{CH}_3)_2\text{Ga} : \text{NH}_2]_3$ and GaN molecules respectively. Lastly, Equation 9 depicts the incorporation of nitrogen on substrate from ammonia.

	Surface reactions
1	$(\text{CH}_3)_3\text{Ga} + \text{S} \rightarrow \text{Ga}(\text{s}) + 3\text{CH}_3$
2	$(\text{CH}_3)_2\text{Ga} + \text{S} \rightarrow \text{Ga}(\text{s}) + 2\text{CH}_3$
3	$(\text{CH}_3)\text{Ga} + \text{S} \rightarrow \text{Ga}(\text{s}) + \text{CH}_3$
4	$\text{Ga} + \text{S} \rightarrow \text{Ga}(\text{s})$
5	$(\text{CH}_3)_3\text{Ga} : \text{NH}_3 + 2\text{S} \rightarrow \text{GaN}(\text{s}) + 3\text{CH}_4$
6	$(\text{CH}_3)_2\text{Ga} : \text{NH}_2 + 2\text{S} \rightarrow \text{GaN}(\text{s}) + 2\text{CH}_4$
7	$[(\text{CH}_3)_2\text{Ga} : \text{NH}_2]_3 + 6\text{S} \rightarrow 3\text{GaN}(\text{s}) + 6\text{CH}_4$
8	$\text{GaN} + \text{S} \rightarrow \text{GaN}(\text{s})$
9	$\text{NH}_3 + \text{S} \rightarrow \text{N}(\text{s}) + 1.5\text{H}_2$

Table 3-3. Surface reactions for GaN growth in MOCVD.

3.2.2. Review of MOCVD design

The purpose of MOCVD is to provide a facilitating environment for epitaxial growth of high quality crystalline materials. It is carefully designed to provide the most suitable growth environment, characterized in terms of parameters such as temperature, pressure of gas flow, speed of gas flow, uniformity of temperature distribution etc. These parameters are coupled together and would have impact on each other. For example, the gas flow in MOCVD chamber determines the

distribution of precursor within the chamber, and will have a key impact on the distribution of heat and pressure. Understanding and simulating these parameters to the highest fidelity achievable could provide us a more accurate image of the growth dynamics and mechanisms of GaN within MOCVD. In this thesis, rotating-disk vertical MOCVD will be analyzed in detail, because it is used for GaN growth in this work, and it is also an important category of reactor in the research community.

The rotating susceptor in a rotating-disk MOCVD plays a critical role in generating laminar flows within the reactor, and thus creating suitable distributions of temperature, pressure and precursor for GaN growth. The study of flow generated by a rotating infinite disk in an infinite fluid is pioneered by von Karman. (Kármán, 1921) The approach is to use a similarity transformation to convert the three-dimensional Navier-Stokes partial differential equations to a one-dimensional ordinary differential equation boundary value problem. The rotating disk acts like a centrifugal pump, drawing precursors injected from inlets above towards the disk. Precursors are then spread evenly over the susceptor surface, as shown in Figure 3-2 below. Over the disk, a uniform thickness boundary layer is formed. The boundary layer could be visualized as a layer of precursors moving at the same speed relative to the spinning susceptor. It balances with convection effect induced by the heated susceptor surface, and improves uniformity of material grown.

When considering a realistic reactor with finite-radius disk, the dimensions of disk and chamber have to be significantly larger than the thickness of boundary layer. Furthermore, the reactor has to be designed as a "flow-through" system, allowing gases spinning off the disk to leave the reactor, and thus preventing recirculation in the chamber. (Breiland & Evans, 1991) There are also studies focusing on improving and optimizing the injection concentration and speed of alkyl injection systems of MOCVD, with the aim of improving growth uniformity and efficiency. (Kadinski *et al.*, 2004)

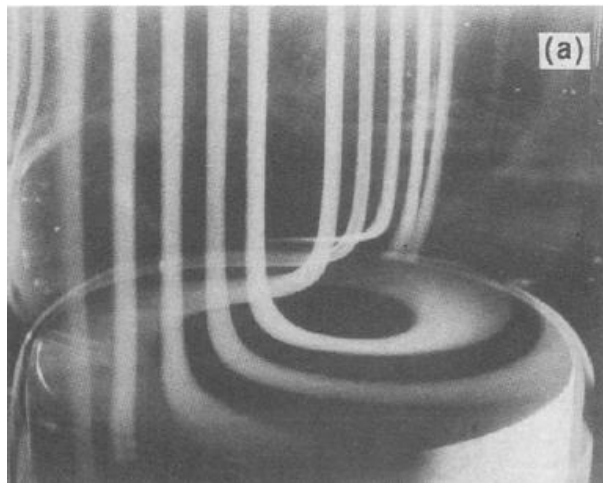


Figure 3-2. Gas flow visualization in a rotating disk MOCVD reactor chamber. (Breiland & Evans, 1991)

3.3. Simulation of GaN growth on Si (100) substrates patterned with V-grooves in COMSOL

3.3.1. Setup of COMSOL simulation

COMSOL's Chemical Reaction Engineering Module is an extension package of COMSOL Multiphysics[®]. It is tailored for the modeling of chemical reaction

systems, with customized physics interfaces and functionalities for the study of phenomena like chemical reactions, mass transport, thermodynamic properties, etc. It is a perfect simulation platform for GaN growth in MOCVD reactor, because it is equipped with in-built mathematical and physical models capable of characterizing important phenomena happening within the MOCVD reactor, including mass transport, fluid flow, heat transfer etc. The interfaces relevant to MOCVD modeling include Chemistry, Fluid Flow and Heat Transfer.

The overall flow of simulation for MOCVD growth of GaN is summarized in Figure 3-3.

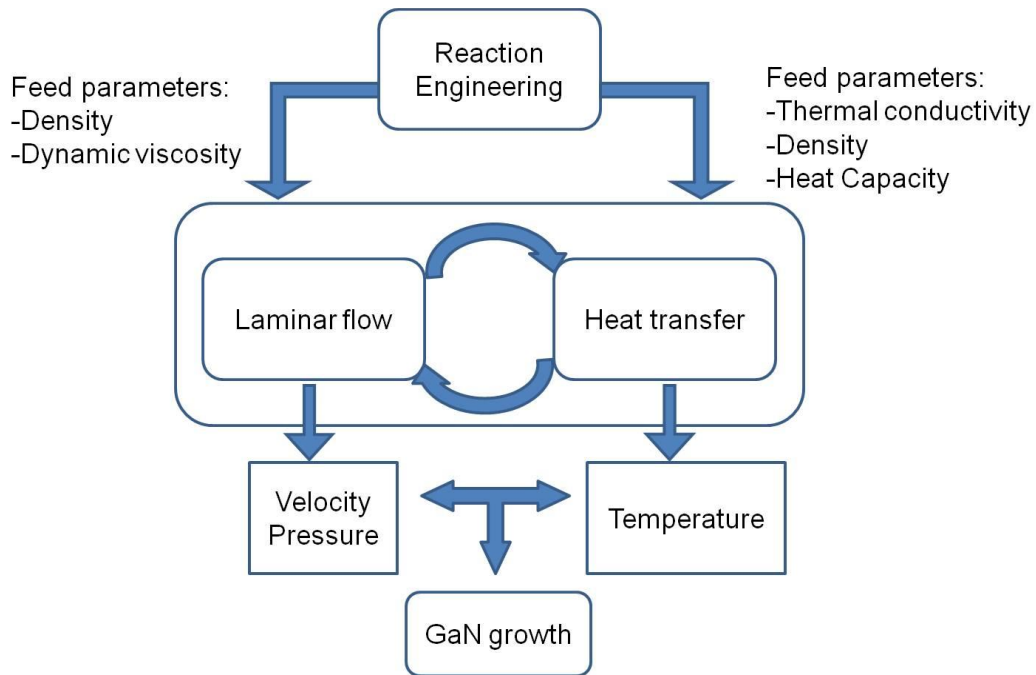


Figure 3-3. Simulation flow chart using COMSOL to study the growth of GaN on V-groove-patterned Si (100) substrates.

Firstly, reaction equations of GaN growth are entered into the Reaction Engineering interface. The aim is to calculate important transport and thermodynamic parameters of the mixed batch reactor. Then, a space-dependent model is generated to incorporate chemical reactions into a physical geometry with real specifications of the EMCORE D180 reactor chamber. Afterwards, the growth dynamics during GaN growth in the reactor is simulated. The detailed modeling setup and results will be explained in sections below.

(a) Reaction Engineering Interface

The Reaction Engineering Interface is designed for modeling chemical reactions and material transport. In order to simulate GaN growth reactions, equations listed in Section 3.2.1 are keyed into the Reaction Engineering Interface. Reaction parameters such as activation energies and rate constants are based on values reported by Parikh et al. in a review article and references therein.(Parikh & Adomaitis, 2006) The interface would assume that the reactor is perfectly mixed, and calculate important parameters for simulation of laminar flow (density, dynamic viscosity), and heat transfer (thermal conductivity, density, heat capacity at constant pressure).

(b) Fluid Flow Interface

One fundamental design requirement for MOCVD is to provide laminar flows of precursors within the reactor chamber, meaning that gas flows within the chamber are in parallel layers without disturbances among them. Laminar flow also implies that the flow speed is under a critical Reynolds number, at which disturbances would start to grow into turbulences. For laminar flow of fluid, velocity and pressure fields could be calculated in the Laminar Flow node under Fluid Flow Interface in COMSOL. The approach is to solve Navier-Stokes equations and continuity equation. The former equation is based on conservation of momentum, and the latter is based on conservation of mass.

The continuity equation in COMSOL is written in the form

$$\frac{\partial \rho}{\partial t} + \nabla \cdot (\rho \vec{u}) = 0 \quad (\text{Eq 3.1})$$

The form of Navier-Stokes Equation for compressible flow in COMSOL is written as

$$\rho \frac{\partial \vec{u}}{\partial t} + \rho \vec{u} \cdot \nabla \vec{u} = -\nabla p + \nabla \cdot \{ \mu (\nabla \vec{u} + (\nabla \vec{u})^T) - \frac{2}{3} \mu (\nabla \cdot \vec{u}) \vec{I} \} + \vec{F} \quad (\text{Eq 3.2})$$

In Equation 3.2 above, ρ is density (kg/m^3); \vec{u} is velocity vector (m/s); p is pressure (Pa); μ is dynamic viscosity (Pa.s); \vec{I} is the identity matrix; \vec{F} is the volume force vector (N/m^3).

Proper boundary conditions have to be set for the computation domain in Laminar Flow Interface, as shown in Figure 3-4. On the top of the reactor, there are eight

inlets for injection of precursors. In COMSOL, the “Inlet” option is used to define conditions at gas injection points. The inlet can be set as either a pressure condition or a velocity condition, while the velocity condition is more robust. In this case, the inlet speed is set at 0.4 m/s, and the direction of injection is vertically downwards. At the bottom of the reactor, two outlets are responsible for guiding waste gases out of the reactor. In COMSOL, the “Outlet” boundary option is prescribed as a pressure constraint via a normal stress condition.

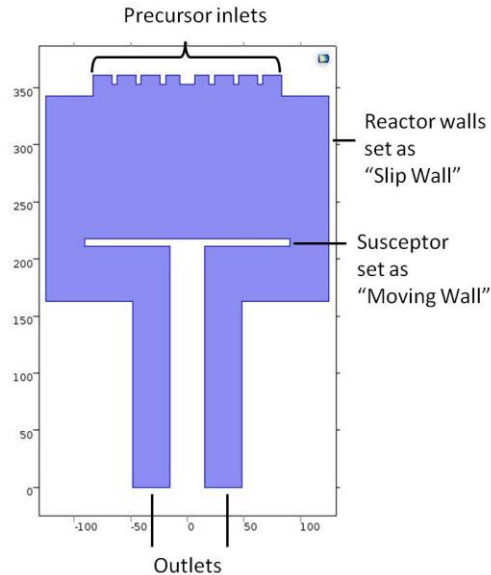


Figure 3-4. Setup in Laminar Flow Interface.

In COMSOL, the "Wall" option is used to define flow conditions at various boundaries and surfaces within the reactor. The "Slip Wall" option describes wall boundaries which have the main purpose of containing reactants within the domain. This condition implies the absence of boundary layer formation and other viscous effects at the wall. Thus, the reactor walls other than inlets and outlets are set as “Slip Wall”. The rotating susceptor is set as "Moving Wall", which is used

in COMSOL to model moving surfaces. The susceptor rotation speed is set to be 1500 rpm.

(c) Heat Transfer Interface

The MOCVD growth process is carried out in an environment of elevated temperature. The precise control of temperature is crucial for ensuring crystal quality. In EMCORE D180 MOCVD, the tungsten-based alloy heating element consists of one inner and one outer filament, embedded below the susceptor. In this simulation, the substrate and susceptor are assumed to be at the same growth temperature, instead of adding a separate heating component, in order to facilitate calculation. The initial temperature of reactor walls and interior are set at 300K denoted by "Temperature 1" in Figure 3-5, while the substrate is set at the growth temperature of GaN denoted by "Temperature 2".

After setting the temperatures, Heat Transfer in Fluid Interface of COMOSL is used to model the temperature distribution within the reactor chamber. The fundamental law governing heat transfer is the principle of conservation of energy, or termed as the First Law of Thermodynamics. The heat transfer equation could be written in terms of internal energy, but internal energy is not a parameter convenient for measurement. Thus in COMSOL, the heat transfer equation is written in terms of temperature as:

$$\rho C_p \left(\frac{\partial T}{\partial t} + (\vec{u} \cdot \nabla) T \right) = -(\nabla \cdot \vec{q}) + \vec{\tau} : \vec{S} - \frac{T}{\rho} \frac{\partial \rho}{\partial T} \Big|_p \left(\frac{\partial p}{\partial t} + (\vec{u} \cdot \nabla) p \right) + Q \quad (\text{Eq 3.3})$$

In Equation 3.3 above, ρ is the density; C_p is the specific heat capacity at constant pressure; T is the absolute temperature; \vec{u} is the velocity vector; \vec{q} is the heat flux by conduction; P is pressure; τ is the viscous stress tensor; \vec{S} is the strain-rate tensor; Q contains heat sources other than viscous heating.

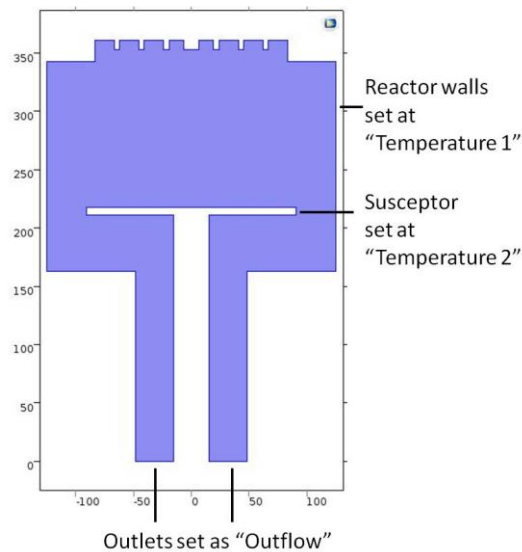


Figure 3-5. Setup in Heat Transfer in Fluids Interface of COMSOL.

Solving the heat transfer equation above for temperature distribution requires setting up proper boundary conditions. The “Outflow” option is used to define the boundary condition at the outlet. The "Outflow" option is suitable for convection-dominated heat transfer. It specifies that at the outlet, the temperature gradient in the normal direction is zero, and radiation is absent.

The setups of Laminar Flow and Heat Transfer modules have to be linked, because the phenomena of laminar flow and heat transfer in a MOCVD chamber are coupled together. In COMSOL, the Multiphysics node is designed to feed computation results from one physics interface to another, catering to simulations involving coupled physics systems such as MOCVD. A "Temperature Coupling" option under Multiphysics node is added to the simulation setup. Heat Transfer Interface is set as the "Source", and Laminar Flow Interface is selected as the "Destination". A "Flow Coupling" is also added, and the selection of source and destination is the reverse.

3.3.2. COMSOL simulation results

In order to investigate the impact of patterned V-grooves of substrate on the growth of GaN in MOCVD, a reference simulation run is first conducted for growth of GaN on flat substrates in COMSOL. Then, GaN growth on substrates patterned with V-grooves is simulated to compare with the flat substrate case. For maximum accuracy, the exact three-dimensional (3D) reactor dimensions should be used for simulation. In 3D simulation, substrates with V-groove alignment directions of 0° , 45° and 90° with respect to the direction of precursor flow could be all simulated to verify the experiment results in Chapter 2. However, computation time for the simulation setup above in 3D geometry is immense. A single run could easily cost hours on a Dell T7500 workstation. Such detailed setup is not suitable for an initial study of a new phenomenon, which requires many test runs. Thus, in order to make the study more efficient, the scope of

Chapter 3 in this master thesis is chosen to be a 2D simulation for the case of V-grooves placed at 90° angle to radial precursor flow. This case could suitably represent the impact of V-grooves on GaN growth dynamics.

For experiments in Chapter 2, the dimensions of V-groove on wafer is 4 μm wide and 100 μm long, separated by 4 μm from each other by silicon nitride mask. The Si (111) facet makes an angle of 54.7 degrees to the horizontal, and the groove depth is 2.82 μm . When such dimensions are used for simulation, there is no discernible impact on the velocity and pressure distributions. This is due to the limitation of COMSOL in mesh size. Such limitation would not prohibit the effort to gain a deeper understanding of the impact of surface groove placement direction on growth mechanisms and the final morphology of GaN. Furthermore, in many cases of GaN growth on patterned substrates, the magnitude of surface depression is much larger than the dimensions used in Chapter 2. Thus, the dimension of V-groove chosen for simulation has an opening width of 4 mm and a depth of 2.82 mm, as illustrated in Figure 3-6 below. The wafer and susceptor are assumed to be an entity, due to the small thickness of the wafer.

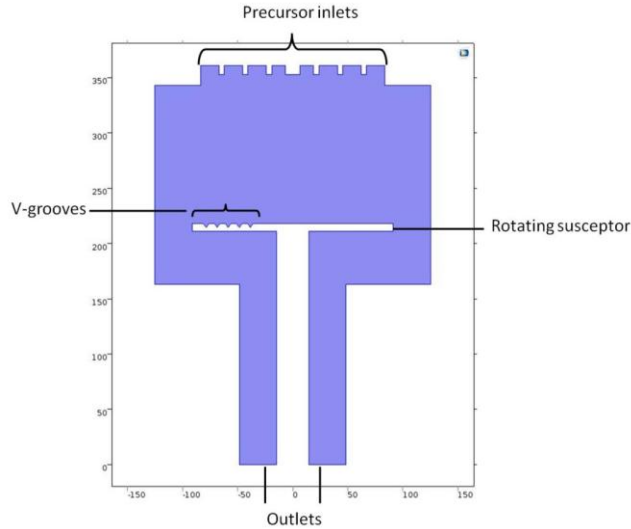


Figure 3-6. Geometry setup for reactor chamber loaded with substrate patterned with V-grooves.

3.3.3. COMSOL simulation results

3.3.3.1. Velocity magnitude distributions

The velocity distribution in reactor loaded with flat substrate is plotted in Figure 3-7 below. There are a number of important observations, which could serve as validations to the simulation model used. Firstly, at the edge of the rotating susceptor, the velocity of precursor is much larger than that in other parts of the reactor. This is firstly due to the fact that precursor gases are being forced through a narrow opening between the susceptor and reactor walls to reach outlets below. Moreover, the heating element below the susceptor has caused precursor gases to increase in temperature and expand in volume. This further increases the amount of gas flow and its velocity through the narrow opening. Secondly, the velocity of precursors directly above the susceptor is slightly higher than that further above. This indicates the formation of a distinct layer of precursor that has a slightly

different velocity. This layer matches the characteristic of a boundary layer, which moves at a speed close to that of the rotating susceptor, and could be visualized as relatively stationary to susceptor. Besides above-mentioned validations, the velocity simulation model is carefully calibrated by comparing to other reports in the literature. (Tseng *et al.*, 2015) Lastly, the conditions on inlet velocity and rotating speed of susceptor are varied in a trend, and the resulting changes on velocity distribution are checked if they are reasonable.

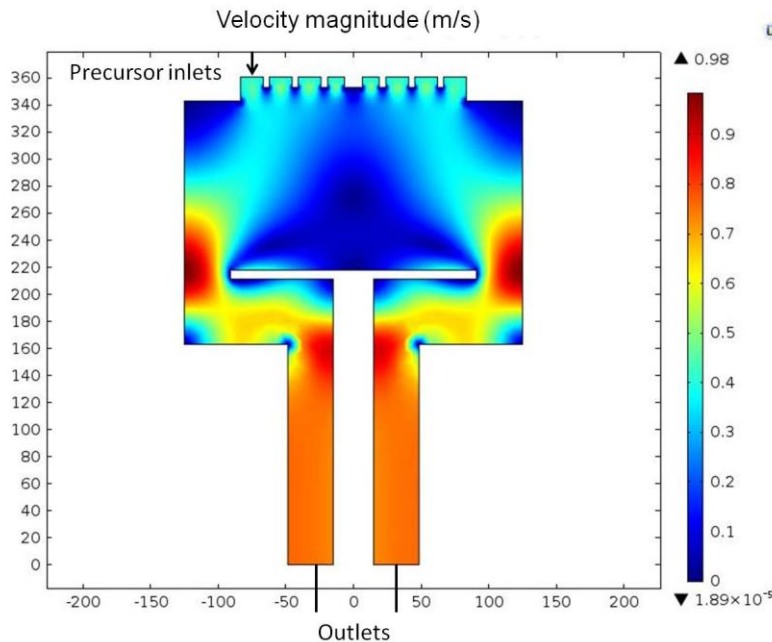


Figure 3-7. Velocity magnitude distribution within reactor chamber loaded with flat substrates.

For reactors loaded with V-groove patterned substrate, the velocity distribution is presented in Figure 3-8 below. A distinctive observation compared to the case of flat substrates is that the velocity of precursors immediately above the V-grooves has become slower. The presence of V-grooves has altered the symmetry of velocity distribution above the susceptor. A number of reasons are speculated to

be the cause. Firstly, the V-grooves would trap precursors within them, and thus creating a "dragging" effect on precursors passing over the V-grooves. Furthermore, if equi-velocity contours are plotted over the V-grooves, the direction of flow is from the right facet of V-groove to the outer reactor chamber. This directed flow would not be disturbed due to the absence of a precursor layer with slightly larger velocity over the V-grooves. This directed flow of precursor away from the right facet would improve the chance of growth on the other facet of V-grooves. This could be one factor contributing to the single-facet growth on V-grooves observed in Chapter 2.

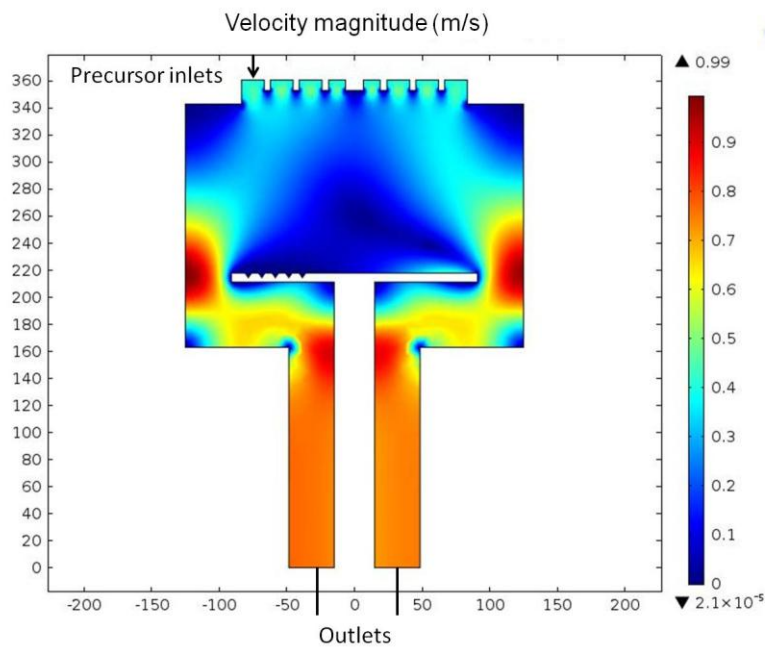


Figure 3-8. Velocity magnitude distribution within reactor chamber loaded with V-grooves-patterned substrate.

3.3.3.2. Pressure distributions

Next, pressure distributions within the reactor chamber loaded with both flat and V-groove-patterned substrates are presented. For flat substrate, the pressure distribution within the reactor is symmetrical as shown in Figure 3-9 (a).

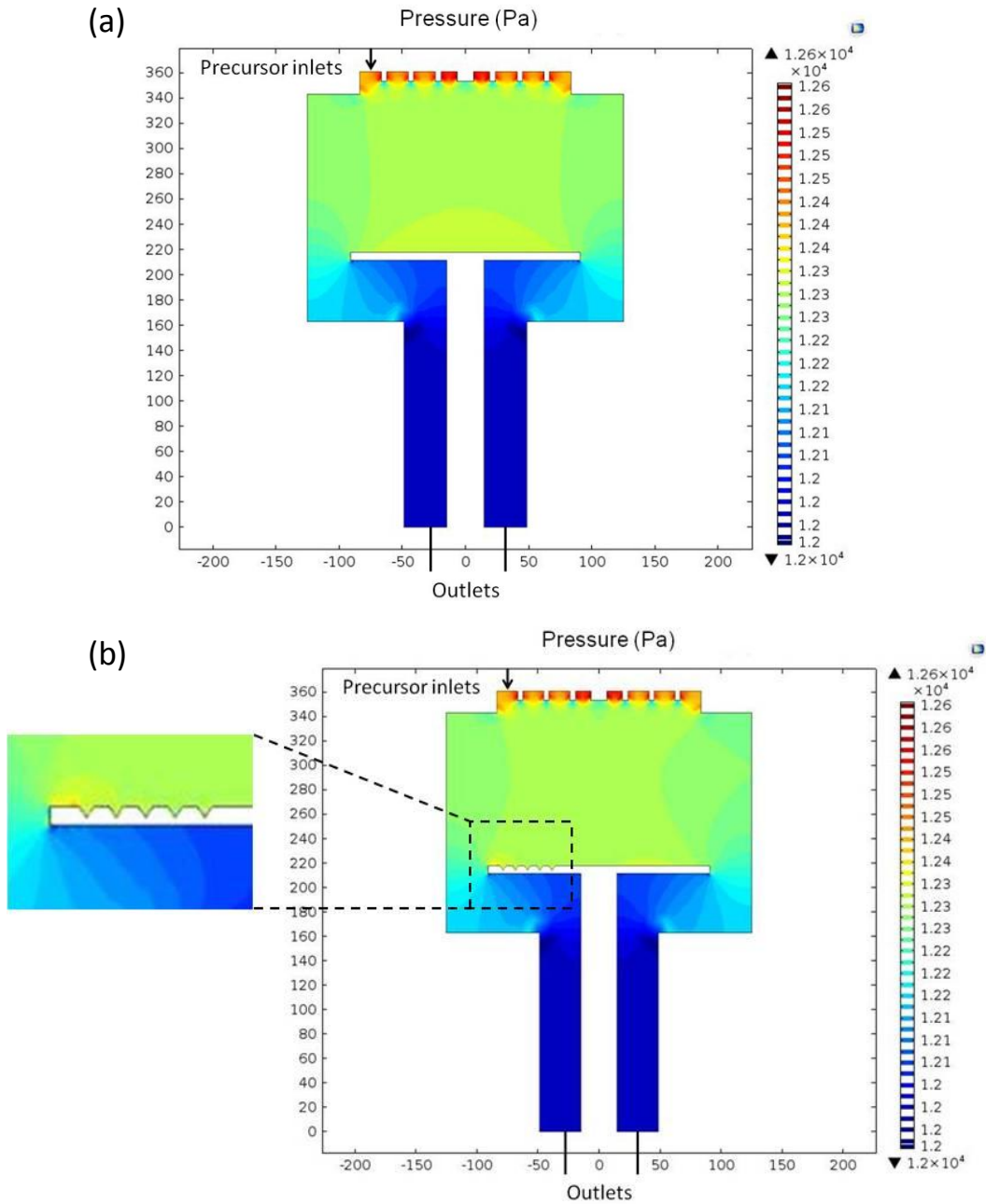


Figure 3-9. Pressure distributions in reactor chamber loaded with (a) flat and (b) V-groove-patterned substrates.

On the contrary, the pressure distribution for substrate with patterned V-grooves is asymmetrical as shown in Figure 3-9 (b). Upon close examination of the enlarged inlet, for V-grooves near the left end of susceptor, there is a region of higher pressure directly above the left-side facets, compared to pressure over the right-side facets.

The effect of pressure on growth rate of GaN in MOCVD is widely studied. (Hirako *et al.*, 2005) This effect is more pronounced in vertical MOCVD with rotating-disk. The chamber pressure would significantly affect the thickness of boundary layer which is generated by the rotating disk, and in turn affect the growth rate. In a report by Kadinski *et al.*, the growth rate of GaN increases from 1.2 $\mu\text{m/h}$ to 2.3 $\mu\text{m/h}$, when the growth pressure is increased from 100 torr to 400 torr. (Kadinski *et al.*, 2004) In terms of physics explanation, an increase in growth pressure would increase the residence time of precursors. Furthermore, the probability of intermolecular collisions would increase, and the mean free path would decrease. (Dauelsberg *et al.*, 2007) In mathematical terms, the relationship between pressure and adsorption rate could be written as

$$R_i^S = F_i \cdot S = \frac{P}{(2\pi M_i R_{gas} T)^{0.5}} \cdot x_i \cdot S \quad (\text{Eq 3.4})$$

In Equation 3.4 above, R_i^S is the adsorption rate of i th species; F_i is the flux of i th species arriving at the surface; M_i is the molecular weight; R_{gas} is the ideal

gas constant; T is absolute temperature; x_i is the mole fraction of species i above the surface; S is sticking probability.

The expression of flux F_i is derived from the kinetic theory of gases, and it is governed by Hertz-Knudsen Equation. (Kolasinski & Kolasinski, 2012) It could be seen that pressure is directly proportional to the gas flux and adsorption rate. Thus, the observation of higher pressure over the left-side facets of V-grooves in Figure 3-9 (b) is related to a higher product of gas flux and adsorption rate on the left facet. A higher product of gas flux and adsorption rate is a contributing factor for preferable growth of GaN on one of the two V-groove facets, when the V-grooves are placed perpendicular to the direction of precursor flow.

3.3.3.3. Temperature distributions

The following section will present simulations of temperature distributions within MOCVD chamber loaded with flat and V-groove patterned substrates. Chemical reactions leading to the growth of GaN are heavily dependent on temperature. Temperature not only determines reaction rates, but also the sequence of gas phase reaction pathways. For example, one study on the effect of heating on gas phase reactions has revealed that higher temperature would make direct pyrolysis of TMG a preferable pathway compared to decomposition via intermediate products. (Zuo *et al.*, 2012) Other studies also reveal that a change in the temperature distribution, even a small amount, will affect the concentration of

growth species on the growth surface. (Hirako & Ohkawa, 2005) In this report by Hirako et al., the simulation finds that the decomposition of TMG into $(\text{CH}_3)_2\text{Ga}$ and $(\text{CH}_3)_2\text{Ga}$ (as listed in Equations 1 and 2 in Table 3-1) will be almost complete at temperatures around 800 K. Then, the decomposition of $(\text{CH}_3)_2\text{Ga}$ and formation of Ga atoms (Equation 3 in Table 3-2) require a higher temperature than 800 K. Thus, larger amount of Ga atoms will be generated at higher-

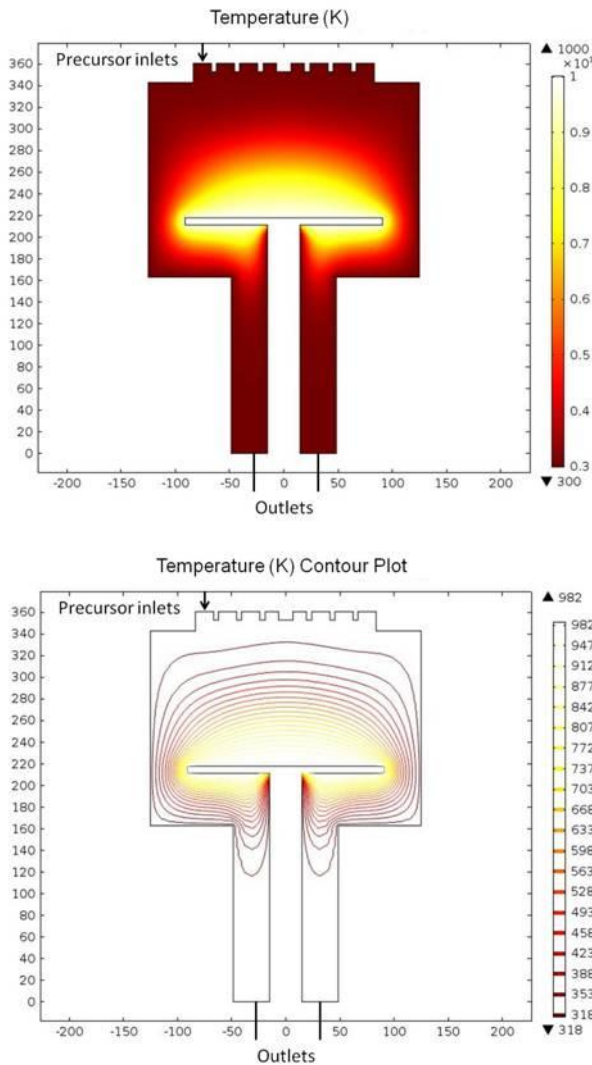


Figure 3-10. Temperature distribution (a) and contour plot (b) in reactor chamber loaded with flat substrates.

temperature regions. The maximum amount is more likely to be generated at the outer circumferential regions, which are usually at the highest temperature.

In this thesis, the simulation of temperature distributions is computed by the Heat Transfer Interface in COMSOL. For the case of flat substrate, the temperature distribution and temperature contour diagrams are plotted in Figure 3-10. From the temperature distribution and contour plot, it could be seen that the heating element would create a

significant radiation field within the reactor chamber.

The temperature and contour plots for reactor loaded with substrates patterned with V-grooves are shown in Figure 3-11. There are no discernible changes compared to the case of flat substrate. This might be due to the fact the radiation

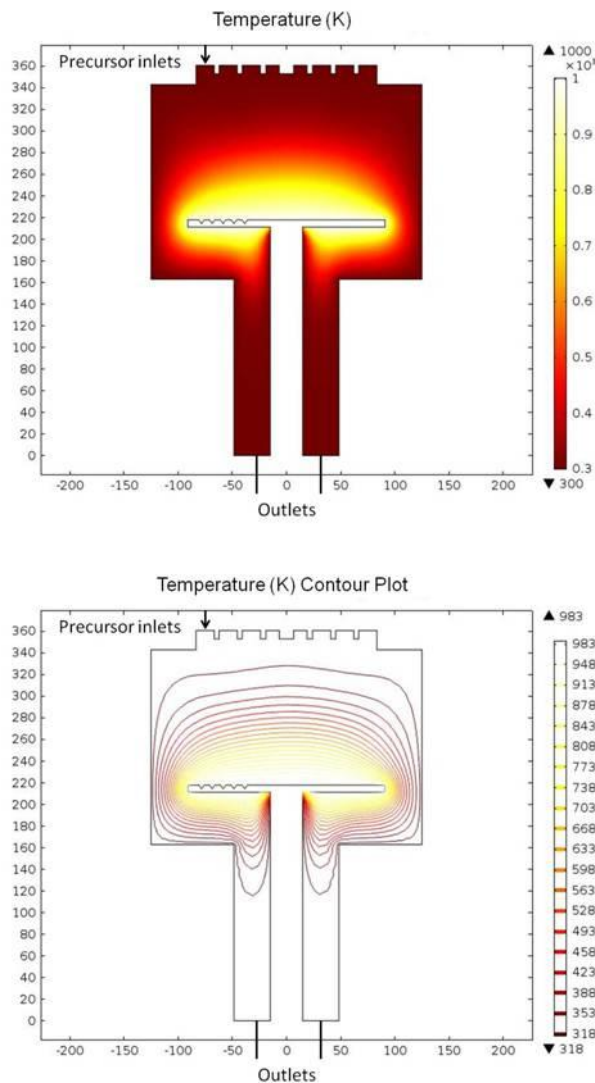


Figure 3-11. Temperature distribution (a) and contour plot (b) in reactor chamber loaded with V-groove patterned substrates.

field from the heating element is intense, and changes induced by the presence of V-grooves are subtle or obscured by the high radiation field.

In order to better understand the effect of V-grooves on temperature distributions within a MOCVD reactor chamber, a hypothetical study is performed next. The heat capacity of gases within the reactor chamber is arbitrarily increased by ten times. This

deviation from realistic

parameters could serve as a test run for an initial study of surface depressions' effect on the temperature distribution within a reactor chamber. The resulting temperature and contour plots are shown in Figure 3-12 below.

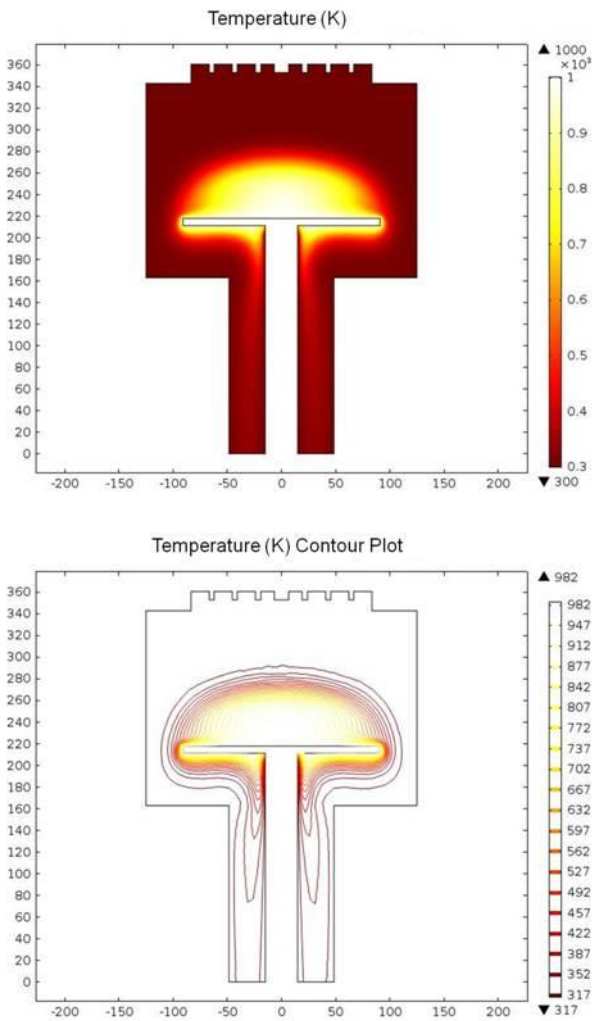


Figure 3-12. For hypothetical study of higher specific heat capacity of precursor, temperature distribution (a) and contour plot (b) in reactor chamber loaded with flat substrates.

It could be seen that the temperature distribution is still symmetrical, but the radiation field directly above the susceptor edges has been reduced.

When the reactor chamber is loaded with V-groove patterned substrate, the temperature distribution and contour plot is presented in Figure 3-13. The temperature distribution has become asymmetrical. One region above the flat part of the substrate is of lower temperature. The temperature contours are more loosely

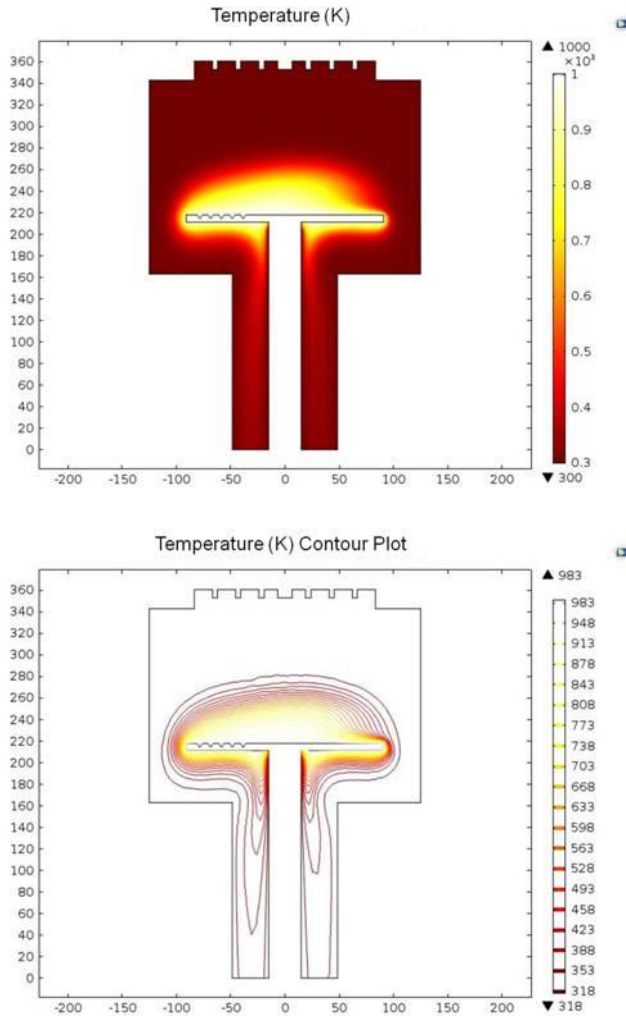


Figure 3-13. For hypothetical study of higher specific heat capacity of precursor. Temperature distribution (a) and contour plot (b) in reactor chamber loaded with V-grooves-patterned substrates.

spaced compared to the region above V-grooves. This temperature gradient would cause the heat flux to be tilted towards the region above V-grooves. This observation could be linked to the observation in velocity distribution, that velocity above the V-grooves is slower than that above the flat part of substrate. The higher temperature region above the V-grooves would induce a more facilitating environment for the growth of GaN, especially for the decomposition of $(\text{CH}_3)\text{Ga}$ into Ga atoms, which require a higher temperature than 800 K.

In summary, the effect of V-grooves on distributions of velocity, pressure and temperature within the reactor chamber have been simulated in this chapter. The slower velocity above V-grooves and flow flux directly away from the right-side facets would induce preferable growth on the left-side facets. Moreover, a higher pressure region is observed over the left-side V-groove facets. This increase in pressure is linked to a higher product of gas flux and adsorption rate through the Hertz-Knudsen Equation. These factors will make single-facet growth of GaN more favorable. Even though the simulation of heat transfer has not revealed significant differences between the cases of flat and V-groove patterned substrates, the role of heat transfer in facilitating single-facet growth should not be deemed negligible. A hypothetical study with increased gas heat capacity has revealed that the presence of surface V-grooves could disturb the symmetry of temperature distribution, and induce a region of lower temperature above the flat part of substrate. Its detailed effect on growth dynamics of GaN could be performed in future study.

Chapter 4 Proposed integration of single-photon emitter with optical fiber in cascaded V-grooves on Si (100) substrate

4.1. Motivation

4.1.1. Overview

The advance of GaN-on-Si technology has enabled the monolithic integration of logic switching, optoelectronics and photonics devices on one silicon platform. Compared to previous integration techniques such as flip-chip or wafer-bonding assemblies, monolithic integration of GaN with Si-based devices offers benefits such as denser and more efficient wafer layout, reduction of interconnect size and losses. For logic switching application, the integration of CMOS and HEMT is widely studied. (Hoke *et al.*, 2012) For optoelectronic application, the integration usually involves a light source based on III-V semiconductors, and silicon-based photonic devices such as modulators and couplers. (Chilukuri *et al.*, 2006)

One cutting-edge and promising future application of GaN-on-Si integration technology for optoelectronic application is in the field of non-classical light generation. The reasons are two-fold. Firstly, GaN-based quantum dots have been demonstrated to be able to generate single photons at higher temperatures, compared to other single-photon emitters which usually require cryogenic operation temperatures. In a report by Kako *et al.* (Kako *et al.*, 2006), hexagonal GaN / AlN quantum dots grown by Stranski–Krastanov mode on a (0001)-

oriented 6H-SiC substrate have been demonstrated to generate single photons at an operation temperature of 200K. It is a promising single-photon source in the blue to ultraviolet region of spectrum. This spectral region is particularly interesting for quantum-optical applications, as a shorter wavelength of photons could reduce the size of transmitters and receivers. Kako et al. have attributed the higher operation temperature of the single-photon emitter to a number of special properties of the GaN / AlN quantum dot system, including high optical-phonon energies and pronounced quantum-confinement effect.

An inherent problem relating to the process of non-classical light generation is that the coupling and guiding of non-classical light generated are difficult and unpredictable. These problems arise due to the ultra-small size of non-classical light generator. The second reason for the application of GaN-on-Si technology for non-classical light generation is that it offers a solution to the above problem. GaN-based non-classical light emitter could be monolithically integrated with Si-based photonic devices or an optical fiber, and achieve easier and more predictable coupling and guiding of photons generated. In this thesis, a non-classical light emitting and coupling system based on GaN-on-Si platform is proposed and verified in simulation. A schematic of the proposed device structure is illustrated in Figure 4-1. The blue prism is the light emitting structure fabricated by method reported in Chapter 2. Then an optical fiber is embedded within a larger V-groove cascaded to the smaller V-groove containing the light source.

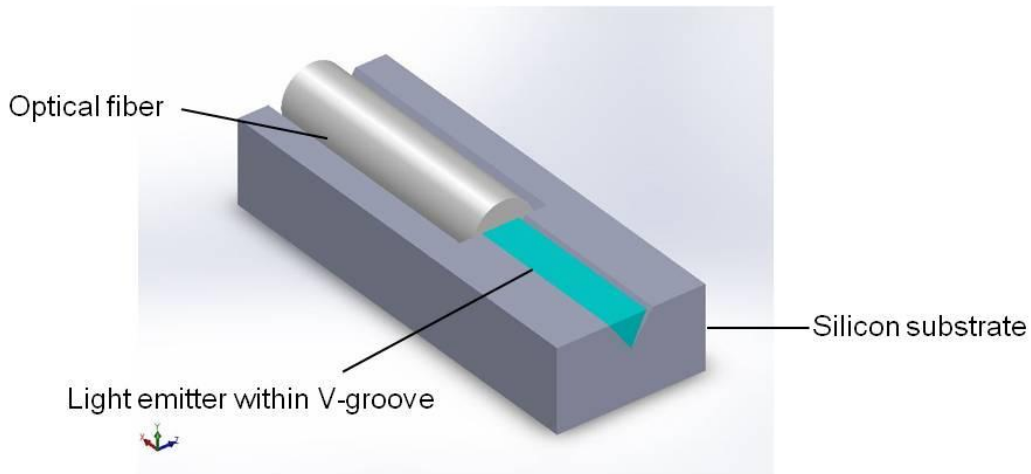


Figure 4-1. Proposed device structure consisting of a single-photon source and an optical fiber, embedded within cascaded V-grooves on Si (100) substrate.

In the literature, there are yet to be reports on single-photon emitters fabricated within V-grooves patterned on Si (100) substrate, based on author's best knowledge. Nonetheless, fabrication of classical light sources such as LEDs has been achieved within the V-grooves patterned on Si (100) substrate. For example, Reuters et al. have fabricated semi-polar green and blue (1-101) InGaN / GaN QW-based LEDs within V-groove trenches patterned on Si (100) substrate. (Reuters *et al.*, 2015) The device structure is shown in Figure 4-2. In another report by Kushimoto et al., (1-101) InGaN / GaN MQWs are also fabricated on Si (111) facets of V-grooves etched on Si (100) substrate. The difference is that the QWs are enclosed within a cavity structure, which consist of two inner GaN waveguides and two outer AlGaN cladding layers. With the confinement effect of the cavity structure, optically-pumped lasing is achieved. (Kushimoto *et al.*, 2015) References would be made to these reports in simulation and analysis below, in order to validate the proposed structure.

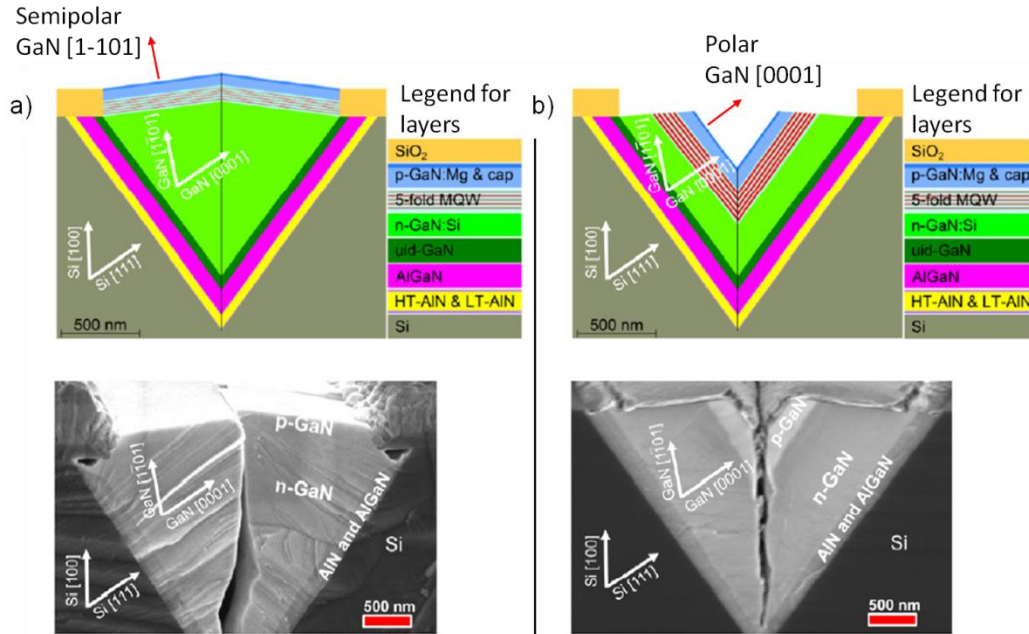


Figure 4-2. (a) Semipolar (1-101) InGaN/GaN LED grown on Si (111) facets of V-grooves patterned on Si (100) substrate. (b) Reference LED on polar (0001) plane. (Reuters *et al.*, 2015)

4.1.2. Introduction to non-classical light generation

4.1.2.1. Non-classical light

Light could be classified according to its intensity correlation characteristics into categories of bunched light, coherent light, and anti-bunched light. Figure 4-3 provides a simplified visualization of the distinct characteristics of various types of light sources. For bunched light, photons would arrive in groups. For coherent light source, photons arrive at random intervals. For anti-bunched light, photons arrive at regular intervals between them.

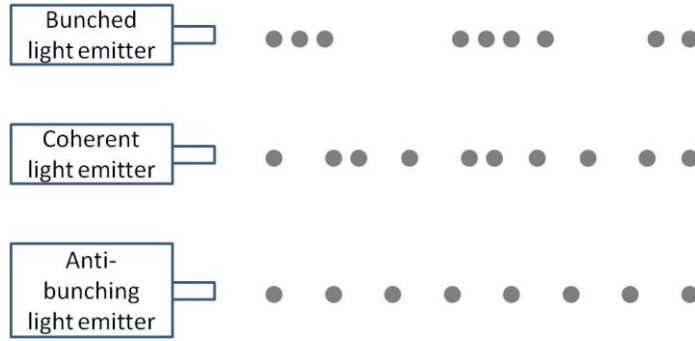


Figure 4-3. Illustration for photon streams in different types of light sources.

In order to quantify the characteristic of non-classical light sources, second-order correlation function is used. It is defined as:

$$g^{(2)}(\tau) = \frac{\langle \varepsilon^*(t)\varepsilon^*(t+\tau)\varepsilon(t+\tau)\varepsilon(t) \rangle}{\langle \varepsilon^*(t)\varepsilon(t) \rangle \langle \varepsilon^*(t+\tau)\varepsilon(t+\tau) \rangle} = \frac{\langle I(t)I(t+\tau) \rangle}{\langle I(t) \rangle \langle I(t+\tau) \rangle} \quad (\text{Eq. 4.1})$$

In Eq. 4.1 above, $\varepsilon(t)$ is the electric field of light at time t ; $I(t)$ is the intensity of light at time t .

Table 4-1 below summarizes the corresponding values of the second-order correlation function at zero time delay for different types of light. Also, the classical equivalent descriptions for various types of light are listed.

Types of light	$g^{(2)}(0)$	Classical Description
Bunched	>1	Chaotic
Coherent (Random)	1	Coherent
Anti-bunched	<1	No classical equivalent

Table 4-1. Classification of light based on photon arrival intervals, and corresponding values of second-order correlation functions and classical descriptions. (Fox, 2006)

One thing to note is that anti-bunched light does not have a classical equivalent description, because it is a purely quantum phenomenon.

One special type of anti-bunched light sources is single-photon emitter. In idealistic situation, a single-photon source should produce exactly one photon in response to an external trigger. The emitted photon could then be modulated in terms of its polarization or other properties and carry information. Due to the indivisibility of photon and the invasive nature of quantum system measurement, tapping on communication link using single photons as information-carriers would cause the wave functions of photons to collapse and the information will be lost. (Fox, 2006) Thus, single-photon emitter is a crucial component for applications of quantum cryptography (Gisin *et al.*, 2002), quantum communication and quantum information processing (Monroe, 2002).

In order to measure the value of second-order correlation function and judge the performance of a single-photon emitter, Hanbury Brown and Twiss setup (HBT) is used. (Brown & Twiss, 1957; Brown & Twiss, 1958) A schematic of the HBT setup is shown in Figure 4-4. In the setup, photons emitted from an emitter are fed into a beam splitter and split into two paths, each connecting to a photon detector.

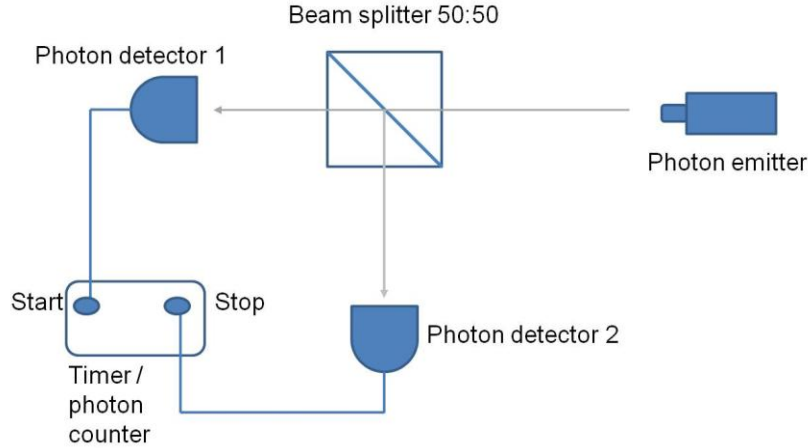


Figure 4-4. Hanbury Brown and Twiss setup for measuring second-order correlation function.

The second-order correlation function above is defined in terms of intensity correlations. Because the number of photons arriving at a detector is proportional to the intensity of light, the second-order correlation function could be re-written as

$$g^{(2)}(\tau) = \frac{\langle n_1(t)n_2(t+\tau) \rangle}{\langle n_1(t) \rangle \langle n_2(t+\tau) \rangle} \quad (\text{Eq. 4.2})$$

In Eq. 4.2, $n_d(t)$ is the number of counts at detector d at time t . The above expression indicates that, the second-order correlation function is directly related to the probability of detecting photons simultaneously on one photon detector at time t , and on the other detector at time $t + \tau$. (Fox, 2006) The HBT setup is connected to a computer to plot a histogram showing the number of photon detection events happening within a certain time interval. For an ideal single-photon source, there should be no simultaneous photon arrival events on the two photon detectors at a time delay of zero.

4.1.2.2. Single photon source

A number of material systems have been proposed for the purpose of single-photon generation, such as nitrogen-vacancy center in diamond. (He *et al.*, 1993) Among them, single-photon sources based on solid-state quantum dots are an important category of non-classical light emitters. Quantum dot's discrete and optically active energy states have made it a suitable candidate for single-photon emitter. Another advantage of it is that solid-state quantum dots could be relatively easily integrated with passive optical devices such as optical cavities and waveguides. The types of cavities suitable for integration with single-photon sources based on solid-state quantum dots include microdisk cavities, micropillar cavities, photonic crystal cavities, etc. (Vahala, 2003)

The realization of single-photon emitters with electrical pumping is an important development. An electrically driven single-photon source based on self-assembled InAs / GaAs quantum dot is demonstrated by Yuan *et al.* in 2002. (Yuan *et al.*, 2002) The structure consists of InAs quantum dots embedded within a GaAs p-i-n diode. A schematic illustrating the device structure is shown in Figure 4-5. Back-contact method is used for n-ohmic contact. The p-ohmic contact on the top also functions as an aperture, allowing photon emissions from only one quantum dot to be detected, and filtering out emissions from other quantum dots. In another report, self-assembled InAs quantum dots are embedded within a cavity, which provides horizontal confinement of light by an AlO_x layer produced by wet oxidation of aluminum-rich Al_xGa_{1-x}As, as well as vertical confinement of light

by a GaAs / AlGaAs distributed Bragg mirror. (Ellis *et al.*, 2007) The AlO_x layer is also used as an aperture allowing emissions from a single quantum dot to be detected. The design of using an aperture to obtain emission from a single quantum dot has an inherent problem. The alignment of a single quantum dot and the aperture opening is not well controllable and predictable. It requires many time-consuming trial and error experiments. Furthermore, extra effort is required to grow sparsely distributed quantum dots, in order to increase the probability of getting a single quantum dot directly under the aperture.



Figure 4-5. Single-photon emitter structure based on self-assembled quantum dots with electrical pumping. (Yuan *et al.*, 2002)

One approach to solve this problem is to detect the location of a single quantum dot first by cathodoluminescence spectroscopy. Then electron-beam lithography (EBL) is used to define a circular sub-micron mesa containing the single quantum dot. The mesa is subsequently etched, and it would contain a single quantum dot within. (Gschrey *et al.*, 2013)

The proposed single-photon emitter structure in this thesis is embedded within a V-groove trench on Si (100) substrate, and connected to an optical fiber

embedded within a bigger cascaded V-groove. The aim is to achieve predictable single-photon source location and photon coupling. The details of the proposed structure are presented in Section 4.3.

4.2. Area-selective quantum well intermixing and quantum dot fabrication

Quantum well intermixing (QWI) refers to inter-diffusion of atoms across the heterointerface between well layers and boundary layers in quantum wells (QW). As-grown QW structures have well defined boundaries between well regions and barrier regions. When atoms inter-diffuse across these boundaries under the external influence such as heat, the composition profile across the QW structure will be modified. This will lead to changes in bandgap, refractive index and optical absorption coefficient, etc. The techniques used to induce QWI include impurity-free vacancy disordering (IFVD), impurity induced disordering, laser induced disordering and focused ion beam induced intermixing. (Li & Lie, 1998) Among these methods, IFVD has been widely studied for monolithic integration of photonic devices. This is because it provides the advantage of not affecting carrier concentrations and not requiring implantation of impurity atoms which will cause crystal damage.

The bandgap modification induced by QWI could be used to form QDs within QW structures, if the bandgap modification could be restrained within a selected area of QW. In order to achieve area-selective QWI, a commonly used method is to deposit a capping layer on top of the QW region desired for QWI, and subject

the QW to thermal annealing. The cap layer could be dielectric, metal, or dielectric / metal materials. The capping layer will affect the extent of QWI, either promoting or inhibiting it, through two different mechanisms namely diffusion mechanism and thermal stress mechanism.

For AlGaAs / GaAs quantum wells, a dielectric SiO₂ capping layer is found to induce QWI. (Ooi *et al.*, 1997) The first reason is that Ga atoms possess a high diffusion coefficient in SiO₂ dielectric cap layer at annealing temperatures above 800°C. Rapid thermal annealing (RTA) would induce Ga atoms to out-diffuse into the SiO₂ cap layer, and thus generate group-III vacancies under it. The presence of Ga vacancies in the QW will promote intermixing of Ga atoms with Al atoms, and thus results in blue-shifted emission energy under the cap layer.

The second mechanism responsible for enhanced inter-diffusion under the SiO₂ cap layer is the tensile thermal stress created at the interface between GaAs and SiO₂ layer. Compared to SiO₂, GaAs has a much larger thermal expansion coefficient. At elevated temperatures, GaAs will expand more than the SiO₂ layer on top. The tensile stress in SiO₂ layer will result in broken bonds in it, making it more porous. The presence of more broken bonds in SiO₂ will induce greater out-diffusion of Ga atoms.

On the contrary, SrF₂ cap layer is used to shield and inhibit QWI effect from AlGaAs / GaAs QWs. This is because the diffusion coefficient of Ga atoms is

much lower in SrF₂ layer, and the thermal stress created at SrF₂-GaAs interface during annealing is compressive. The compressive stress would obstruct out-diffusion of Ga atoms. SiO₂ and SrF₂ cap layers could be used in combination to confine QWI in desired parts of a QW structure. This method has been used to create integrated photonic devices. (Yeo *et al.*, 2001)

For InGaN / GaN QWs, reports on selective QWI are limited. This is partly due to the fact that inter-diffusion in InGaN / GaN MQWs is complicated by the immiscibility of GaN and InN. Phase separation is also reported at higher temperatures. In order to induce QWI in InGaN / GaN MQWs, higher temperatures in the range of 1200-1400°C are usually required. Under such high annealing temperatures, a high nitrogen over-pressure in the range of 15 kbar within the RTA chamber is required to prevent surface decomposition. (McCluskey *et al.*, 1998) The use of high temperature and high pressure during annealing process will pose serious challenges in inducing QWI while preserving the material quality.

Recently, the use of dielectric and dielectric/metal layers to achieve area-selective QWI on InGaN / GaN MQWs has been reported in the literature. (Shen *et al.*, 2015) It is found that Molybdenum:SiO₂ capping layer with Mo concentration of 4 atomic-percent could effectively induce intermixing within a LED structure consisting of 12 pairs 3 nm In_{0.2}Ga_{0.8}N well / 13.5 nm GaN barrier QWs. The shift in emission photon energy is about 80 meV after annealing at 950 °C for two

cycles of 120 seconds. In contrast, SiO₂ capping layer could effectively shield QWI effect from QWs. This observation shows an opposite role of SiO₂ cap layer in inhibiting QWI rather than inducing it in InAlGaAs system. The reason is that in the report above, a tensile stress of 140 MPa is obtained in the Mo:SiO₂ capping layer, while a compressive stress is obtained in the SiO₂ dielectric layer. A tensile stress in the Mo:SiO₂ capping layer would induce broken bonds in it and attract Ga atoms to diffuse out. On the contrary, a compressive stress in SiO₂ layer would obstruct the out-diffusion of Ga atoms.

In this work, the single-photon source proposed in this thesis would be based on InGaN / GaN quantum dot (QD). There are several ways to fabricate InGaN / GaN QDs. One approach is strain-induced island growth. (Damilano *et al.*, 1999) This method is relatively easy to operate, but the QDs fabricated are unpredictable in location and emission wavelength. Another approach is to fabricate InGaN / GaN QWs first, and then obtain QDs within QWs through modifications to the QW structure. One type of modification is that on top of a planar single quantum well, pillars with height about 100 nm are fabricated through reactive ion etching. (Zhang *et al.*, 2013) The pillars will each contain a single InGaN nanodisk, functioning as the active region of a quantum dot.

In this thesis, another type of modification through area-selective QWI by thermal annealing is proposed to form QDs within InGaN / GaN QW. On a QW structure, a small region is covered by SiO₂ cap layer. According to Shen *et al.*'s report,

QW structure under SiO₂ cap layer will be shielded from QWI. Then, other parts of the QW structure is covered by Mo : SiO₂ cap layer, which will induce QWI within QW region below and cause an increase in bandgap. QW region under the SiO₂ cap layer will have a smaller bandgap compared to other parts of the QW. If the difference in emission energy is large enough, confinement will be achieved, and a quantum dot is created. The detailed structure is explained below.

4.3. Proposed structure

Two types of photon emitting structures are proposed. For the first type, the demonstrated growth of GaN on Si (111) facet of V-groove patterned on Si (100) substrate in Chapter 2 is performed. Growth time is carefully controlled to allow the main growth direction of GaN to switch from (0001) c-plane direction to (1-101) direction. In other words, the aim is to obtain a GaN prism with a flat top (1-101) plane sufficiently large for device fabrication. Then, a single InGaN / GaN QW with 3 nm wide InGaN well and 10 nm wide GaN barrier is fabricated on the top (1-101) semi-polar plane of the GaN prism grown. The detailed layer stack proposed to be grown on Si (111) facet of V-groove on Si (111) substrate is presented in Figure 4-6.

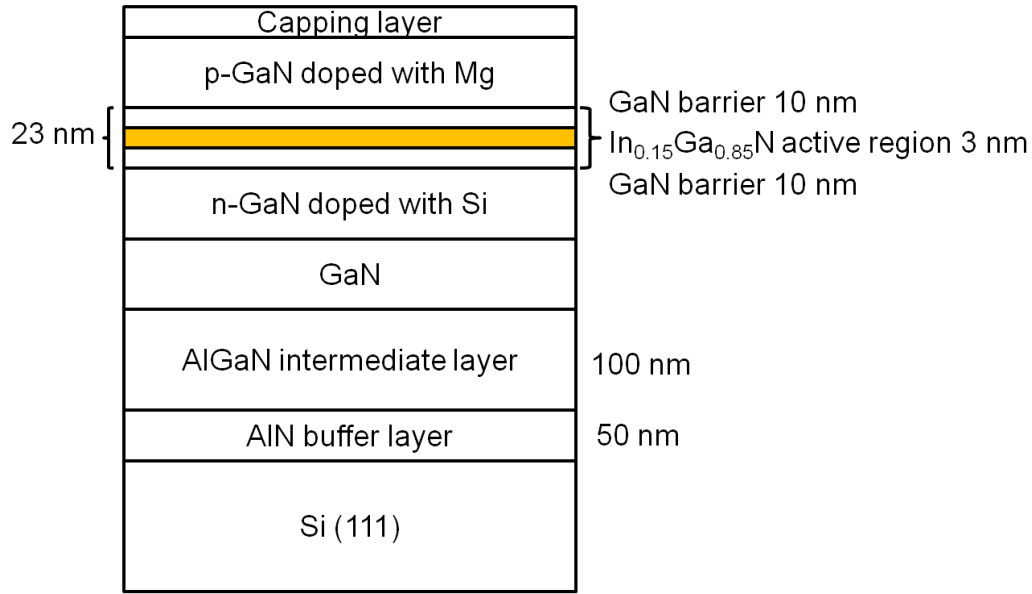


Figure 4-6. Proposed detailed layer stack grown on Si (111) facet of V-groove.

In order to obtain a non-classical light emitter with sufficiently small size, the method of QWI by RTA is proposed to form one quantum dot in the InGaN / GaN quantum well. In order to achieve area-selective QWI, a circular patch-shape SiO₂ layer with a diameter of 200 nm and thickness of 300 nm is proposed to be deposited on top of the QW structure. In Figure 4-7, it is illustrated as a yellow-color circular disk. It is deposited by sputtering and patterned by a standard photolithography lift-off process. Then, a 300 nm thick Mo : SiO₂ capping layer (purple layer in Figure 4-7) is deposited on top of the GaN prism, covering the circular patch-shape SiO₂ cap layer and the entire GaN (1-101) semi-polar plane.

The small region covered by SiO₂ path-shape layer is designed to be non-intermixed when subjected to a rapid thermal annealing at 950 °C for two cycles of 120 seconds. Other parts of the QW structure covered by only Mo:SiO₂ layer is

designed to be intermixed, and a blue-shift in emission photon energy is expected. This design aims to create a small-size region under the SiO₂ cap layer, having a smaller bandgap compared to other parts of the QWs, i.e a QD. Photons emitted from this QD region are of lower energy compared to emission from the intermixed QW region. When these lower-energy photons are travelling through other QW regions with larger bandgap, they would not be absorbed. This is because photons emitted from the QD region do not possess enough energy to excite electrons in intermixed QW regions to jump from one energy level to a higher one.

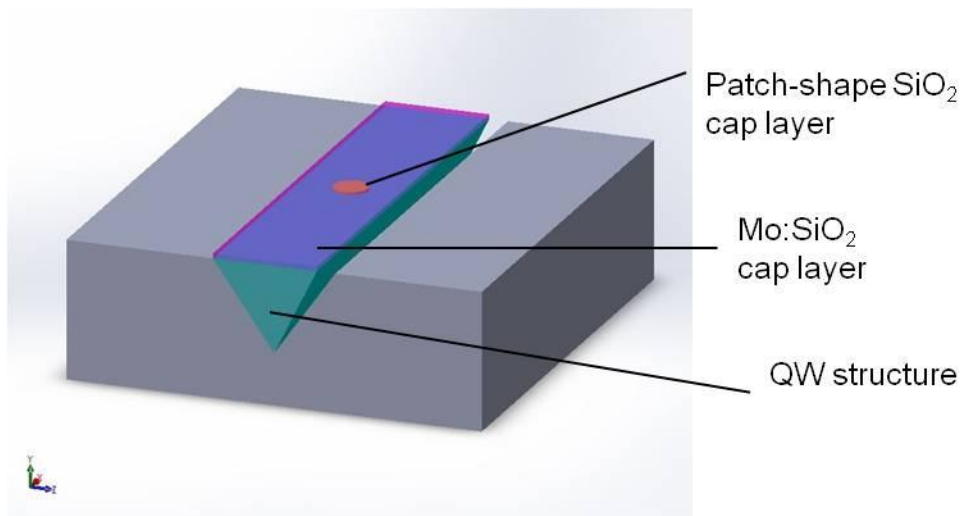


Figure 4-7. Proposed cap layer depositions on semi-polar InGaN / GaN SQW fabricated on Si (111) facet of V-groove.

For the second type of proposed structure, the growth of GaN is stopped while the main growth direction is still in the (0001) c-plane direction. The resulting GaN is of trapezoidal shape, filling half of the V-groove trench (blue region in Figure 4-

8). Then, the above specified SQW structure is grown. The circular patch-shape SiO_2 layer is deposited on the (0001) c-plane. The top (1-101) plane is also covered with SiO_2 dielectric layer (yellow region). Then, a Mo : SiO_2 cap layer (purple region) is deposited on the (0001) plane, covering the patch-shape SiO_2 layer. In the following sections, the proposed structures will be simulated to calculate the change in bandgap after QWI.

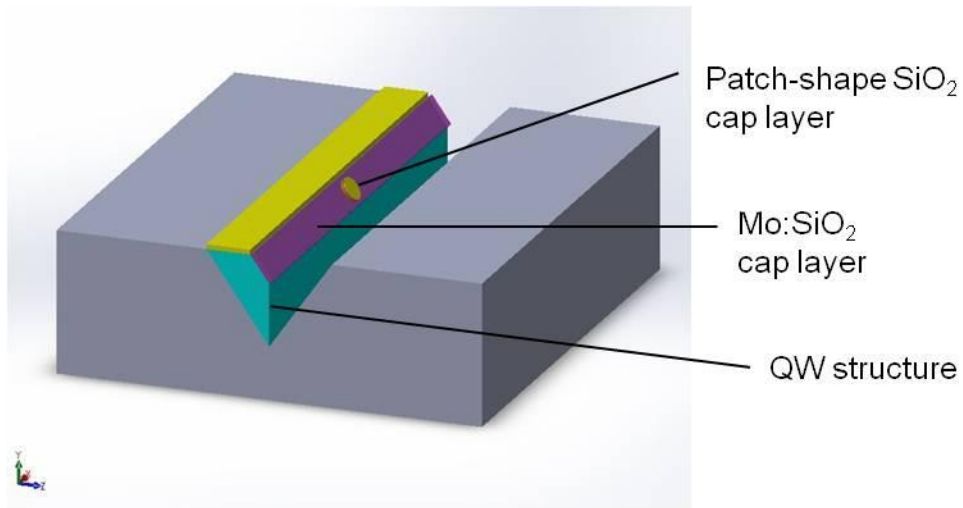


Figure 4-8. Proposed cap layer depositions on polar InGaN / GaN SQW fabricated on Si (111) facet of V-groove.

4.4. Simulation of proposed single-photon emitter with optical fiber in cascaded V-grooves on Si (100) substrate

4.4.1. Fabrication of QD by QWI

The aim of this part of thesis is to validate the proposed method of creating an InGaN / GaN QD within QW by QWI, for the purpose of single-photon emitter.

More specifically, the focus is to simulate the extent of QWI and subsequent shift in emission length in selective region of QW.

The indium profile in the QW structure after QWI is first calculated. Due to the effect of QWI, the concentration profile of indium with respect to diffusion length

(L_d) along the growth direction is governed by the Fick's Law, i.e, $\frac{\partial C}{\partial t} = D \frac{\partial^2 C}{\partial z^2}$.

The solution is an error function (J.Crank, 1980), given by

$$C(z) = \frac{1}{2} C_0 \left[\operatorname{erf} \left(\frac{h-z}{L_d} \right) + \operatorname{erf} \left(\frac{h+z}{L_d} \right) \right] \quad (\text{Eq. 4.1})$$

in which C_0 is the initial concentration of indium; h is half of the well-width; $z = 0$ is the center of well. C_0 used is 15% ($\text{In}_{0.15}\text{Ga}_{0.85}\text{N}$), because it is the indium content easily achievable. $h = 3/2 = 1.5$ nm. L_d is the inter-diffusion length, and can be expressed as $L_d = \sqrt{Dt}$, in which D is diffusion coefficient, and t is annealing time. Its value is set to be the same as in Shen et al.'s report, which is 10 Å.

The indium profile obtained in the intermixed QW region covered with Mo : SiO_2 cap layer is shown in Figure 4-9.

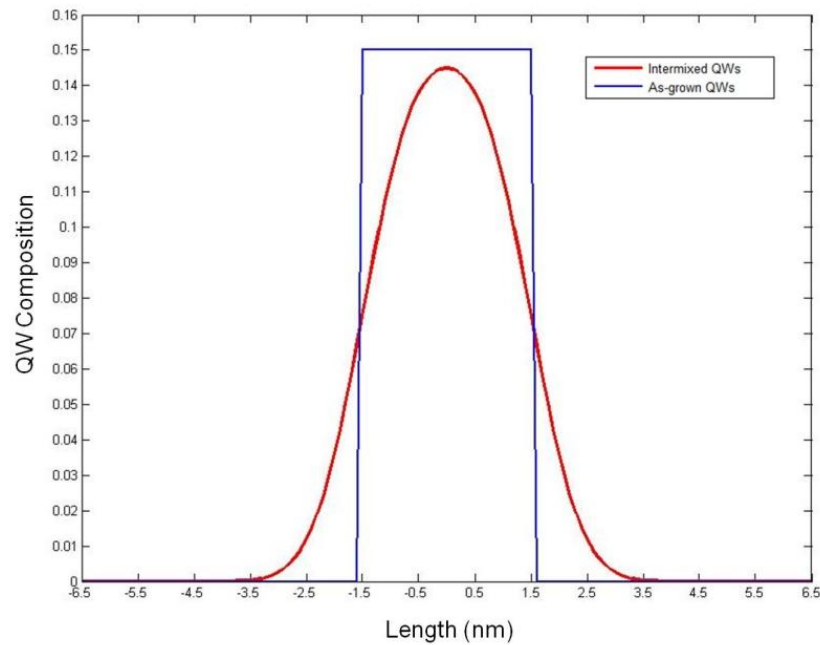


Figure 4-9. Indium composition profile for as-grown QWs (blue), and intermixed QWs (red).

The indium profile is then entered into SILVACO software to calculate the band structure and the shift in emission photon energy after QWI. The way to feed indium profile into SILVACO is to approximate the smooth error function using a piecewise function. In this thesis, it is done by dividing the well width into seven equal parts and finding the average indium content within each part. Then, seven layers of InGaN with the respective average indium content are defined in SILVACO. The setup in SILVACO is included in Appendix A.5.

In SILVACO, the method to calculate QW bandgap and bound state energy is by using classical drift-diffusion solver with self-consistent Schrödinger-Poisson solver. Quantum well bound state energy could be used to calculate spontaneous

emission rate by using effective mass approximation from k.p theory, under parabolic band approximation.

Calculation in SILCACO reveals that the QW bandgap for non-intermixed SQW structure defined in Figure 4-6 is 2.62 eV. For intermixed QW region with inter-diffusion length $L_d = \sqrt{Dt} = 10 \text{ \AA}$, the QW bandgap changes to 2.64 eV. The QW bandgap for intermixed QW region increases by 20 meV, compared to non-intermixed region. Relating this result to the structure design in Figure 4-7 and 4-8, the selectively intermixed region in the QW region covered with Mo:SiO₂ cap layer will produce blue-shifted emissions, while region under the SiO₂ cap layer will not be intermixed and the emission photon energy is not shifted. The blue-shifted emission photons could be filtered out, leaving photons emitted from the QD region under SiO₂ circular patch-shape layer to test for its photon characteristics. In order to achieve single-photon emission, the annealing time needs to be adjusted to obtain the right amount of emission shift within the selectively intermixed region of QW, so that the quantum dot region could have one bound energy state for emission. The simulation model constructed in the work involving QWI modeling and bandgap calculation could be used to corroborate experiments on fabricating single photon emitters within V-grooves on Si (100) substrates.

4.4.2. Coupling with silicon waveguide

It is an inherent problem to couple and guide photons emitted from small structures like QDs in a controllable way. The V-groove-patterned Si (100) substrate provides a platform to solve this problem. To achieve this, the method of wet etching is used to fabricate a bigger-size V-groove cascaded to the smaller V-groove with light emitting device within. Then a single-mode optical fiber is stripped of its outer cladding, and its core section with a diameter of 8 micron is embedded within the bigger V-groove to couple light generated. The air will act as a cladding to allow light in the core to achieve total internal reflection while propagating in it.

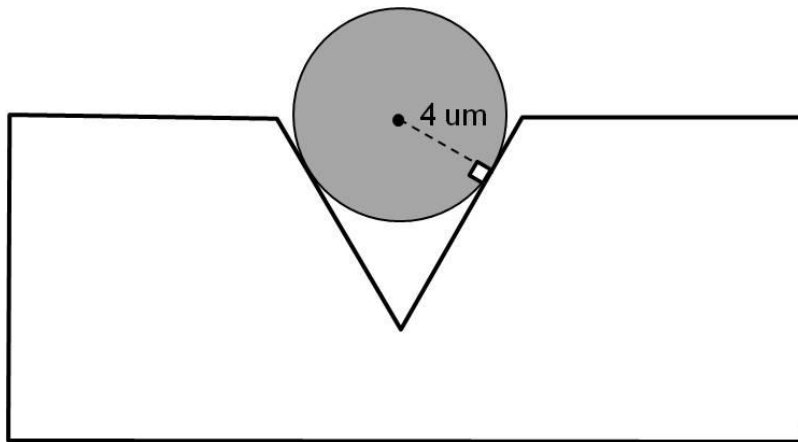


Figure 4-10. Single-mode optical fiber core placed within V-groove patterned on Si (100) substrate.

A few precautions have to be made. Firstly, the wet etching time of the bigger V-groove needs to be carefully controlled. For placement of fiber, the sidewalls of V-grooves are desired to be smooth, in order to ensure tight fitting. Furthermore, the right type of optical fiber should be selected according to the emission

wavelength, in order to minimize absorption and losses. For InGaN / GaN QWs, the emission wavelength is in the blue region, and Thorlabs' SM300 fiber with operating wavelength in the range of 320-430 nm could be used. Lastly, the dimension of the bigger V-groove has to be carefully calculated to ensure that the photons emitted are within the acceptance angle of the optical fiber. Another possibility other than optical fiber is to fabricate a rectangular silicon waveguide connected to the V-groove with photon emitter. However, it is not suitable for this case, as the absorption coefficient of silicon for light in the blue to ultra-violet region is very high.

Chapter 5 Conclusion and future work

5.1 Conclusion

The prime focus of this master thesis has been studying the growth of GaN on V-groove patterned Si (100) substrates, and investigating the issues associated with both material growth and device fabrication. In the experimental part of this thesis, the contribution of this thesis is to study the growth morphology of GaN when V-grooves on Si (100) substrates are placed at different angles to the direction of precursor flow over the susceptor. It is found that by placing the longitudinal axis of V-grooves perpendicular to the direction of radial precursor flow, single-facet growth of GaN on V-groove is obtained. This observation is corroborated by the cases of 45° and 0° placements. When V-grooves are placed at 45° to the direction of precursor flow, two prisms which differ in size are obtained. When V-grooves are placed in parallel to precursor flow, no growth is observed. This systematic study suggests that there could exist a relationship between V-groove placement direction relative to precursor flow and growth morphology of GaN. This observation offers a more convenient method to obtain single-facet growth of GaN on V-grooves patterned on Si (100) substrate, compared to the method of masking one facet with silicon oxide using Glancing Angle Deposition equipment.

The second contribution of this thesis is to study the dynamics of GaN growth on V-groove patterned Si (100) substrates. A simulation model has been set up in

COMSOL software to incorporate precursor flow and heat transfer effects within the reactor together. The presence of V-grooves has disturbed the symmetries in distributions of precursor flow velocity and pressure. A region of higher pressure is observed over one of the two facets of V-grooves on Si (100) substrate. This increase in pressure would cause an increase in gas flux and adsorption rate through the Hertz-Knudsen Equation, thus facilitating GaN growth. The simulation also reveals that the impact of V-grooves on the temperature distribution is more pronounced for precursors with higher specific heat capacity.

Lastly, a single-photon emitting and coupling structure within the V-groove of Si (100) substrate is proposed and simulated to validate its feasibility. The light source is proposed to be an InGaN / GaN QD formed within SQW. Selective QWI in region of the SQW covered by Molybdenum : SiO₂ capping layer will result in a region of larger bandgap, while the small region covered by SiO₂ circular patch cap is shielded from QWI, and becomes a region of smaller bandgap. To calculate the amount of bandgap shift in intermixed QW region, a simulation model is set up in SILVACO. It reveals that for a diffusion length of 10 Å, QWI will result in an increase of 20 meV in bandgap. This simulation platform could be used to compute shift in bandgap as a result of QWI, and guide the planning of experiments which utilize QWI as the method to create QD for application in single-photon generation.

5.2 Future work

The growth of GaN on patterned Si substrate is a powerful technique to enable the integration of III-nitride semiconductor and Si electronics. In this work, the simulation of growth dynamics is conducted for a 2D model of MOCVD reactor, instead of a 3D simulation. Simulation is performed for only the case of V-grooves placed at 90° to precursor flow direction. This is because 3D simulation requires large computation power, as it involves a much detailed geometry. In future work, 3D simulation could be performed for GaN growth on V-grooves placed at other angles to the direction precursor flow direction. Also, atomic assembly simulation could also be performed to study the actual growth of GaN.

In the last part of this thesis, a single-photon emitting and coupling structure within the V-groove of Si (100) substrate is proposed. The experimental realization of this structure should undergo several stages. Firstly, InGaN / GaN SQW should be grown on Si (111) facets of V-groove patterned on Si (100) substrate. This experiment is already being carried out in our research group. The key to obtain good quality InGaN layer is to precisely control the pressure during growth. The second stage is to deposit cap layers on SQW to define regions for QWI. Firstly, a 200 nm diameter circular patch-shape SiO_2 cap layer is deposited on QW region designed to be non-intermixed. Then, Molybdenum: SiO_2 cap layer with Mo concentration of 4 atomic-percent is deposited on QW region designed to be intermixed. The precise deposition of SiO_2 patch-shape capping layer requires Glancing Angle Deposition System. The last step is to thermally anneal the

sample. Due to the high annealing temperature close to 1000°C, multiple cycles of annealing are expected to prevent decomposition of material. Photoluminescence mapping will be used to reveal the extent and spatial variation of QWI. In order to test whether the area-selective QWI is able to create a region of QD, low temperature PL is needed. Simulation model in this work could provide a guideline for the annealing temperature and time, and assist experiment planning and result analysis.

Bibliography

References in Chapter 1

DADGAR, A. et al. Metalorganic chemical vapor phase epitaxy of crack-free GaN on Si (111) exceeding 1 μm in thickness. Japanese Journal of Applied Physics, v. 39, n. 11B, p. L1183, 2000.

GUHA, S.; BOJARCZUK, N. A. Multicolored light emitters on silicon substrates. Applied physics letters, v. 73, n. 11, p. 1487-1489, 1998.

ISHIKAWA, H. et al. Thermal stability of GaN on (111) Si substrate. Journal of crystal growth, v. 189, p. 178-182, 1998.

KROST, A.; DADGAR, A. GaN-Based Devices on Si. physica status solidi (a), v. 194, n. 2, p. 361-375, 2002.

KUSHIMOTO, M. et al. Optically pumped lasing properties of InGaN/GaN stripe multiquantum wells with ridge cavity structure on patterned (001) Si substrates. Applied Physics Express, v. 8, n. 2, p. 022702, 2015.

LI, T.; MASTRO, M.; DADGAR, A. III-V Compound Semiconductors: Integration with Silicon-Based Microelectronics. CRC press, 2010.

Mo, C., Fang, W., Pu, Y., Liu, H., and Jiang, F. Growth and characterization of InGaN blue LED structure on Si(111) by MOCVD. Journal of Crystal Growth 285 (2005):312–317.

REUTERS, B. et al. Selective MOVPE of InGaN-based LED structures on non-planar Si (111) facets of patterned Si (100) substrates. Journal of Crystal Growth, v. 391, p. 33-40, 2014.

REUTERS, B. et al. Semi-polar {1-101} blue and green InGaN/GaN light-emitting diodes on micro-stripe patterned Si (1 0 0). Journal of Physics D: Applied Physics, v. 48, n. 48, p. 485103, 2015.

Wan, J., Venugopal, R., Melloch, M. R., Liaw, H. M., & Rummel, W. J. Growth of crack-free hexagonal GaN films on Si (100). *Applied Physics Letters*, 79(10), 1459-1461, 2001.

References in Chapter 2

CARTIER, E.; STATHIS, J. H.; BUCHANAN, D. A. Passivation and depassivation of silicon dangling bonds at the Si/SiO₂ interface by atomic hydrogen. *Applied Physics Letters*, v. 63, n. 11, p. 1510-1512, 1993.

ISHIKAWA, H. et al. Thermal stability of GaN on (111) Si substrate. *Journal of crystal growth*, v. 189, p. 178-182, 1998.

LIN, K.-L. et al. Growth of GaN film on 150 mm Si (111) using multilayer AlN/AlGaN buffer by metal-organic vapor phase epitaxy method. *Applied Physics Letters*, v. 91, n. 22, p. 22211-1, 2007.

Long, R. D., & McIntyre, P. C. (2012). Surface preparation and deposited gate oxides for gallium nitride based metal oxide semiconductor devices. *Materials*, 5(7), 1297-1335.

MORKOÇ, H. Handbook of nitride semiconductors and devices, *Materials Properties, Physics and Growth*. John Wiley & Sons, 2009.

NI, X. et al. Non-polar m-plane GaN on patterned Si (112) substrates by metalorganic chemical vapor deposition. *OPTO*, International Society for Optics and Photonics. p.760220-760220-8, 2010.

OLESINSKI, R. W.; KANANI, N.; ABBASCHIAN, G. J. The Ga-Si (Gallium-Silicon) system. *Bulletin of Alloy Phase Diagrams*, v. 6, n. 4, p. 362-364, 1985.

ROMANOV, A. et al. Strain-induced polarization in wurtzite III-nitride semipolar layers. *Journal of Applied Physics*, v. 100, n. 2, 2006.

SAWAKI, N. et al. Growth and properties of semi-polar GaN on a patterned silicon substrate. *Journal of Crystal Growth*, v. 311, n. 10, p. 2867-2874, 2009.

TAKEUCHI, T. et al. Optical properties of strained AlGa_xN and GaInN on GaN. Japanese journal of applied physics, v. 36, n. 2B, p. L177, 1997.

TANAKA, S. et al. Transmission electron microscopy study of the microstructure in selective-area-grown GaN and an AlGa_xN/GaN heterostructure on a 7-degree off-oriented (001) Si substrate. Japanese journal of applied physics, v. 41, n. 7B, p. L846, 2002.

TANIKAWA, T. et al. Growth of non-polar (112̄ 0) GaN on a patterned (110) Si substrate by selective MOVPE. Journal of Crystal Growth, v. 310, n. 23, p. 4999-5002, 2008.

YAO, T.; HONG, S.-K. Oxide and nitride semiconductors: Processing, properties, and applications. Springer Science & Business Media, 2009.

ZHANG, N. et al. The effect of the Al_xGa_{1-x}N/AlN buffer layer on the properties of GaN/Si (111) film grown by NH₃-MBE. Journal of crystal growth, v. 280, n. 3, p. 346-351, 2005.

References in Chapter 3

ALMOND, M. J. et al. Organometallic precursors to the formation of GaN by MOCVD: structural characterisation of Me₃GaNH₃ by gas-phase electron diffraction. Journal of organometallic chemistry, v. 439, n. 3, p. 251-261, 1992.

BREILAND, W. G.; EVANS, G. H. Design and verification of nearly ideal flow and heat transfer in a rotating disk chemical vapor deposition reactor. Journal of the Electrochemical Society, v. 138, n. 6, p. 1806-1816, 1991.

CHEN, C. et al. Parasitic reactions between alkyls and ammonia in OMVPE. MRS Proceedings, 1995, Cambridge Univ Press. p.103.

DAUELSBERG, M. et al. Modeling and process design of III-nitride MOVPE at near-atmospheric pressure in close coupled showerhead and planetary reactors. Journal of crystal growth, v. 298, p. 418-424, 2007.

HIRAKO, A.; KUSAKABE, K.; OHKAWA, K. Modeling of reaction pathways of GaN growth by metalorganic vapor-phase epitaxy using TMGa/NH₃/H₂ system: a computational fluid dynamics simulation study. Japanese journal of applied physics, v. 44, n. 2R, p. 874, 2005.

HIRAKO, A.; OHKAWA, K. Effect of thermal radiation and absorption in GaN-MOVPE growth modeling on temperature distribution and chemical state. *Journal of crystal growth*, v. 276, n. 1, p. 57-63, 2005.

KADINSKI, L. et al. Computational analysis of GaN/InGaN deposition in MOCVD vertical rotating disk reactors. *Journal of crystal growth*, v. 261, n. 2, p. 175-181, 2004.

KIM, C. S. et al. Numerical and Experimental Study on Metal Organic Vapor-Phase Epitaxy of InGaN / GaN Multi-Quantum-Wells. *Journal of fluids engineering*, v. 130, n. 8, p. 081601, 2008.

KOLASINSKI, K. W.; KOLASINSKI, K. K. *Surface science: foundations of catalysis and nanoscience*. John Wiley & Sons, 2012.

KÁRMÁN, T. V. Über laminare und turbulente Reibung. *ZAMM-Journal of Applied Mathematics and Mechanics/Zeitschrift für Angewandte Mathematik und Mechanik*, v. 1, n. 4, p. 233-252, 1921.

LOBANOVA, A. et al. Effect of V/III ratio in AlN and AlGaN MOVPE. *Journal of crystal growth*, v. 287, n. 2, p. 601-604, 2006.

MITROVIC, B. et al. Reactor design optimization based on 3D modeling of nitrides deposition in MOCVD vertical rotating disc reactors. *Journal of crystal growth*, v. 289, n. 2, p. 708-714, 2006.

MONNERY, W. et al. Ammonia pyrolysis and oxidation in the Claus furnace. *Industrial & engineering chemistry research*, v. 40, n. 1, p. 144-151, 2001.

PARIKH, R. P.; ADOMAITIS, R. A. An overview of gallium nitride growth chemistry and its effect on reactor design: Application to a planetary radial-flow CVD system. *Journal of crystal growth*, v. 286, n. 2, p. 259-278, 2006.

PAWLOWSKI, R. et al. Fundamental models of the metalorganic vapor-phase epitaxy of gallium nitride and their use in reactor design. *Journal of Crystal Growth*, v. 221, n. 1, p. 622-628, 2000.

THOMPSON, A. G. et al. The scaling of CVD rotating disk reactors to large sizes and comparison with theory. *Journal of electronic materials*, v. 25, n. 9, p. 1487-1494, 1996.

THON, A.; KUECH, T. F. High temperature adduct formation of trimethylgallium and ammonia. *Applied physics letters*, v. 69, n. 1, p. 55-57, 1996.

Tseng, C. F., Tsai, T. Y., Huang, Y. H., Lee, M. T., & Horng, R. H. Transport phenomena and the effects of reactor geometry for epitaxial GaN growth in a vertical MOCVD reactor. *Journal of Crystal Growth*, 432, 54-63, 2015.

Zhou, X. W., Murdick, D. A., Gillespie, B., & Wadley, H. N. G. Atomic assembly during GaN film growth: Molecular dynamics simulations. *Physical Review B*, 73(4), 045337, 2006.

ZUO, R. et al. Influence of gas mixing and heating on gas-phase reactions in GaN MOCVD growth. *ECS Journal of Solid State Science and Technology*, v. 1, n. 1, p. P46-P53, 2012.

References in Chapter 4

BROWN, R. H.; TWISS, R. Interferometry of the intensity fluctuations in light II. An experimental test of the theory for partially coherent light. *Proceedings of the Royal Society of London A: Mathematical, Physical and Engineering Sciences*, 1958, The Royal Society. p.291-319.

BROWN, R. H.; TWISS, R. Q. Interferometry of the intensity fluctuations in light. I. Basic theory: the correlation between photons in coherent beams of radiation. *Proceedings of the Royal Society of London A: Mathematical, Physical and Engineering Sciences*, 1957, The Royal Society. p.300-324.

CHILUKURI, K. et al. Monolithic CMOS-compatible AlGaInP visible LED arrays on silicon on lattice-engineered substrates (SOLES). *Semiconductor Science and Technology*, v. 22, n. 2, p. 29, 2006.

DAMILANO, B. et al. Room-temperature blue-green emission from InGaN/GaN quantum dots made by strain-induced islanding growth. *Applied Physics Letters*, v. 75, n. 24, p. 3751-3753, 1999.

ELLIS, D. et al. Oxide-apertured microcavity single-photon emitting diode. *Applied physics letters*, v. 90, n. 23, p. 233514, 2007.

FOX, M. *Quantum optics: an introduction*. OUP Oxford, 2006.

GISIN, N. et al. Quantum cryptography. *Reviews of modern physics*, v. 74, n. 1, p. 145, 2002.

GSCHREY, M. et al. In situ electron-beam lithography of deterministic single-quantum-dot mesa-structures using low-temperature cathodoluminescence spectroscopy. *Applied Physics Letters*, v. 102, n. 25, p. 251113, 2013.

HE, X.-F.; MANSON, N. B.; FISK, P. T. Paramagnetic resonance of photoexcited N-V defects in diamond. II. Hyperfine interaction with the N 14 nucleus. *Physical Review B*, v. 47, n. 14, p. 8816, 1993.

HOKE, W. et al. Monolithic integration of silicon CMOS and GaN transistors in a current mirror circuit. *Journal of Vacuum Science & Technology B*, v. 30, n. 2, p. 02B101, 2012.

J.Crank, *Mathematics of Diffusion*. Oxford Univ. Press, Mar. 1980.

KAKO, S. et al. A gallium nitride single-photon source operating at 200 K. *Nature materials*, v. 5, n. 11, p. 887-892, 2006.

KUSHIMOTO, M. et al. Optically pumped lasing properties of InGaN/GaN stripe multiquantum wells with ridge cavity structure on patterned (001) Si substrates. *Applied Physics Express*, v. 8, n. 2, p. 022702, 2015.

LI, E.; LIE, J. *Semiconductor Quantum Well Intermixing—Material Properties and Optoelectronics Applications*. Gordon & Breach, Amsterdam, 1998.

McCluskey, M. D., Romano, L. T., Krusor, B. S., Johnson, N. M., Suski, T., & Jun, J. Interdiffusion of In and Ga in InGaN quantum wells. *Applied physics letters*, 73(9), 1281-1283, 1998.

MONROE, C. Quantum information processing with atoms and photons. *Nature*, v. 416, n. 6877, p. 238-246, 2002.

Ooi, B. S., McIlvaney, K., Street, M. W., Helmy, A. S., Ayling, S. G., Bryce, A. C., March, J.H. & Roberts, J. S. Selective quantum-well intermixing in GaAs-AlGaAs structures using impurity-free vacancy diffusion. *IEEE journal of quantum electronics*, 33(10), 1784-1793, 1997.

PALIK, E. D. *Handbook of optical constants of solids*. Academic press, 1998.

REUTERS, B. et al. Semi-polar {1-101} blue and green InGaN/GaN light-emitting diodes on micro-stripe patterned Si (1 0 0). *Journal of Physics D: Applied Physics*, v. 48, n. 48, p. 485103, 2015.

SHEN, C.; NG, T. K.; OOI, B. S. Enabling area-selective potential-energy engineering in InGaN/GaN quantum wells by post-growth intermixing. *Optics express*, v. 23, n. 6, p. 7991-7998, 2015.

VAHALA, K. J. Optical microcavities. *Nature*, v. 424, n. 6950, p. 839-846, 2003.

Yeo, D. H., Yoon, K. H., Kim, H. R., & Kim, S. J. Integration of waveguide-type wavelength demultiplexing photodetectors by the selective intermixing of an InGaAs-InGaAsP quantum-well structure. *IEEE journal of quantum electronics*, 37(6), 824-829, 2001.

YUAN, Z. et al. Electrically driven single-photon source. *Science*, v. 295, n. 5552, p. 102-105, 2002.

ZHANG, L. et al. Single photon emission from site-controlled InGaN/GaN quantum dots. *Applied Physics Letters*, v. 103, n. 19, p. 192114, 2013.

Appendices

A.1 Biography

(1) August 2009 – July 2013: National University of Singapore, Bachelor of Engineering (Electrical).

A.2 Publication list

(1) “Spatial control of semipolar GaN/InGaN (10-11) epilayer on non-planar single (111) facet of V-grooved Si (100) substrate”, K. K. Ansa-Antwi, Hongfei Liu, *Shiju Li* and Soo Jin Chua. (Manuscript in preparation)

A.3 Participation in international conference

(1) Poster presentation “Anisotropic growth of semipolar InGaN/GaN quantum wells on Si (111) facets of non-planar V-grooved Si (100) substrate due to effect of MOCVD precursor flow direction within V-grooves”. *S.J.Li*, K.K.Ansa-Antwi, B.Z.Wang, H.F.Liu, S.J. Chua. 2015 MRS Fall Meeting, Boston, USA, Nov-Dec 2015.

A.4 Setup in COMSOL

File Model Definitions Geometry Materials Physics Mesh Study Results

Component 2 Add Component Model Parameters Variables Functions Definitions Import Build All LiveLink Geometry Add Material Materials Blank Material Browse Materials Chemistry 1 Add Physics Physics Build Mesh Mesh 1 Compute Study 5 Add Study Study

Model Builder

- slipwallnotinteriorLamHeatTransFlat - Copy-heatOut-fix4-flatheat.mp
 - Global
 - Definitions
 - Materials
 - Component 1 (comp1)
 - Definitions
 - Reaction Engineering (re)
 - Component 2 (comp2)
 - Definitions
 - Geometry 1(2D)
 - Materials
 - Chemistry 1 (chem)
 - Surface Reactions (sr)
 - Transport of Diluted Species (tds)
 - Laminar Flow 1 (spf)
 - Heat Transfer in Fluids 1 (ht)
 - Multiphysics
 - Mesh 1
 - Study 3
 - Step 1: Time Dependent
 - Solver Configurations
 - Study 4
 - Step 1: Stationary Plug Flow
 - Study 5
 - Step 1: Time Dependent
 - Solver Configurations
 - Results
 - Data Sets
 - Views
 - Derived Values
 - Tables
 - Velocity (spf) 1
 - Pressure (spf) 1
 - Wall Resolution (spf) 1
 - Temperature (ht) 1
 - Isothermal Contours (ht) 1
 - Concentration (re)
 - Temperature (re)
 - Concentration (tds)
 - Velocity (spf)
 - Pressure (spf)
 - Wall Resolution (spf) 1
 - Temperature (ht)
 - Isothermal Contours (ht)
 - Export
 - Reports

Settings

Geometry

Build All

Label: Geometry 1(2D)

Units

Scale values when changing units

Length unit: mm

Angular unit: Degrees

Advanced

Default relative repair tolerance: 1E-6

Automatic rebuild

A.5 Setup of InGaN / GaN QW in SILVACO

```
# Define barrier layer
region material=GaN thickness=0.0065 bottom NY=20 name=qb

# Define well layer, which is divided into seven layers with calculated
# average indium content
region material=InGaN thickness=0.0017 compx.top=0 compx.bottom=8e-4
bottom ny=20 name=qb
region material=InGaN thickness=0.0016 compx.top=8e-4
compx.bottom=0.0582407 bottom ny=20 name=qb
region material=InGaN thickness=0.0012 compx.top=0.0582407
compx.bottom=0.14477 bottom ny=20 led qwell name=well
region material=InGaN thickness=0.001 x.compx=0.14477 bottom ny=20 led
qwell name=well
region material=InGaN thickness=0.0012 compx.top=0.14477
compx.bottom=0.0582407 bottom ny=20 led qwell name=well
region material=InGaN thickness=0.0016 compx.top=0.0582407
compx.bottom=8e-4 bottom ny=20 name=qb
region material=InGaN thickness=0.0017 compx.top=8e-4 compx.bottom=0
bottom ny=20 name=qb

# Define barrier layer
region material=GaN thickness=0.0015 bottom NY=20 name=qb
```